Pharm Res (2016) 33:2314–2336
DOI 10.1007/s11095-016-1889-1

EXPERT REVIEW

Recent Advances on Luminescent Enhancement-Based Porous Silicon Biosensors

S. N. Aisyiyah Jenie[1,3] • Sally E. Plush[2] • Nicolas H. Voelcker[1,4]

Received: 4 December 2015 / Accepted: 17 February 2016 / Published online: 25 February 2016

ABSTRACT Luminescence–based detection paradigms have key advantages over other optical platforms such as absorbance, reflectance or interferometric based detection. However, autofluorescence, low quantum yield and lack of photostability of the fluorophore or emitting molecule are still performance-limiting factors. Recent research has shown the need for enhanced luminescence-based detection to overcome these drawbacks while at the same time improving the sensitivity, selectivity and reducing the detection limits of optical sensors and biosensors. Nanostructures have been reported to significantly improve the spectral properties of the emitting molecules. These structures offer unique electrical, optic and magnetic properties which may be used to tailor the surrounding electrical field of the emitter. Here, the main principles behind luminescence and luminescence enhancement-based detections are reviewed, with an emphasis on europium complexes as the emitting molecule. An overview of the optical porous silicon microcavity (pSiMC) as a biosensing platform and recent proof-of-concept examples on enhanced luminescence-based detection using pSiMCs are provided and discussed.

KEY WORDS biosensors · europium · luminescence enhancement · microcavity · porous silicon

Electronic supplementary material The online version of this article (doi:10.1007/s11095-016-1889-1) contains supplementary material, which is available to authorized users.

✉ Nicolas H. Voelcker
nico.voelcker@unisa.edu.au

[1] ARC Centre of Excellence in Convergent Bio-Nano Science and Technology, Future Industries Institute, University of South Australia, Mawson Lakes, SA 5095, Australia

[2] School of Pharmacy and Medical Sciences, University of South Australia, Adelaide, SA 5000, Australia

[3] Research Centre for Chemistry, Indonesian Institute of Sciences, PUSPIPTEK, Serpong, Tangerang, Banten 15314, Indonesia

[4] GPO Box 2471, Adelaide, South Australia 5001, Australia

ABBREVIATIONS

Å	Angstroms
1D	One-dimensional space
Ag	Silver
AgNP	Silver nanoparticles
A_{Ln}, B_{Ln}	Constants for a given lanthanide in the determination of the inner sphere hydration number
APTES	3-aminopropyltriethoxysilane
Au	Gold
AuNP	Gold nanoparticles
Br_2	Bromine
C_{60}	Type of photosensitiser
Cd/Se	Cadmium/Selenium
cDNA	Complementary strand of deoxyribonucleic acid
CdSe/ZnS	Cadmium selenide/zinc sulfide
CEST	Chemical exchange saturation transfer
CH	Hydrocarbon group
CL	Chemiluminescence
Cl_2	Chlorine
Co^{2+}	Cobalt ion
CRET	Chemiluminescence energy transfer
Cy3-DNA, Cy5-DNA	Cyanine labeled deoxyribonucleic acid
cyclen	1,4,7,10-tetraazadodecane
d	Porous silicon film thickness

$D_0 \rightarrow {}^7F_J$, J =0-4	Transition of the electronic states of the europium ion
D_2O	Deuterated water
DBR	Distributed Bragg reflectors
DELFIA	Dissociation-enhanced lanthanide fluorescent immunoassay
DNA	Deoxyribonucleic acid
dns-l-phe	Dansyl-l-phenylalanine
DO3A	1,4,7,10-tetraaza-cyclotetradecane-1,4,7-triacetic acid
DTPA	Diethylenetriaminepentaacetic acid
Dy(III)	Dysprosium ion
E	Energy state
EDTA	Ethylenediaminetetraacetic acid
ELISA	Enzyme-linked immunosorbent assay
ENSAM	Europium nanoparticles for signal enhancement of antibody microarrays
Eu(III)	Europium ion
Eu[tc] complex	Europium tetracycline complex
Eu-PyDC complex	Europium pyridine-3-5-dicarboxylic acid complex
F^-	Fluoride
FITC	Fluorescein isothiocyanate
fM	Femtomolar
fmol/l	Femtomoles per liters
F-P filters	Fabry-Pérot filters
FRET	Fluorescence resonance energy transfer
FWHM	Full width at half maximum
GOX	Glucose oxidase
H layer	High refractive index layer
h^+	Valence band holes
H_2	Hydrogen
H_2O	Water
H_2O_2	Hydrogen peroxide
H_2SiF_6	Hexafluorosilicic acid
HF	Hydrofluoric acid
HRP	Horseradish peroxidase
HSA	Human serum albumin
HTRF	Homogeneous time resolved fluorescence
I_2	Iodine
IgG	Immunoglobulin G
$KHSO_5$	Potassium peroxymonosulfate
k_{nr}	Non-radiative decay rate
L layer	Low refractive index layer
L mol^{-1} cm^{-1}	Molar absorptivity
LDH	L-lactate dehydrogenase
Ln(III)	Lanthanide ion
LOCI	Luminescent oxygen channeling immunoassay
LOD	Limit of detection
m	Spectral order
M	Molar
MMP	Matrix metalloproteinase
MRI	Magnetic resonance imaging
MTTA-Eu(III)	Eu(III)-4′-(10-methyl-9-anthryl)-2,2′:6′,2″-terpyridine-6,6″-diyl]bis(methylenenitrilo) tetrakis(acetate)
n	Refractive index
NADH	Reduced form of nicotinamide-adenine dinucleotide
NADPH	Reduced form of nicotinamide-adenine dinucleotide phosphate
NC	Nanocrystals
ng/l	Nanograms per liters
ng/ml	Nanograms per milliliters
NH	Amine group
NIR	Near infra-red
nm	Nanometers
nM	Nanomolar
O_2	Singlet oxygen
OH	Hydroxyl group
$OH^{\cdot}$	Hydroxyl radical
PARACEST	Paramagnetic CEST agents
pfu/ml	Plaque-forming units per milliliters
pg/mm^2	picograms per millimeters squared
pH	Acidity numeric scale
phen	1,10-phenanthroline
pM	Picomolar
PMT	Photomultiplier tube
ppm	Parts per million
PSA	Prostate specific antigen
PSCM	Porous silicon coupled microcavity
pSi	Porous silicon
pSiMC	Porous silicon microcavity
QD	Quantum dots
Q-factor	Quality factor of the porous silicon microcavity
Q_m	Quantum yield of a molecule in close proximity to a metal
RDE	Radiative decay engineering
Rhodamine B	9-(2-carboxyphenyl)-6-diethylamino-3-xanthenylidene]-diethylammonium chloride
ROS	Reactive oxygen species
S_0	Ground state of electrons
S_1	Excited singlet state of electrons
SEF	Surface enhanced fluorescence
SERS	Surface enhaced Raman scattering
Si	Silicon
$Si(OH)_4$	Silicic acid
SIF	Silver island films

SiO_2	Silicon oxide
Sm(III)	Samarium ion
SPR	Surface plasmon resonance
ssDNA	Single strand of deoxyribonucleic acid
SWNT	Single walled carbon nanotubes
T_1	Excited triplet state of electrons
Tb(III)	Terbium ion
TC	Thermal carbonisation
TETA	1,4,8,11-tetraazacyclo-tetradecane-1,4,8,11-tetraacetic acid
THC	Thermal hydrocarbonisation
TMPyP	5,10,15,20-tetrakis(1-methyl-4-pyridinio)-porphyrintetra(−toluenesulfonate)
TOPO	Tri-n-octylphosphine oxide
TTA	Conjugated base of 2-theonyltrifluoroacetone
TTF	Tetrathiafulvalene
UV	Ultraviolet
Zn(II)	Zinc ion
β-NAD^+	Nicotinamide-adenine dinucleotide
λ	Wavelength
μFEIA	Microfluidic enzyme immunoassay
μm	Micrometers or microns
μM	Micromolar
μs	Microseconds
τ	Luminescence lifetime
τ_m	Luminescence lifetime of a molecule in close proximity to a metal

INTRODUCTION

The definition of a biosensor has been stated by the IUPAC in 1999 as a device, which is capable of providing selective quantitative or semi-quantitative analytical information through electrical, thermal or optical signals using selective biochemical reactions mediated by isolated enzymes, immunosystems, tissues, organelles or whole cells to detect chemical compounds (1–3). The device consists of two basic components: a physicochemical transducer and a biological recognition element (4). With a defined sensitivity, the latter element interprets information from an analyte or biomarker concentration into a chemical or physical output signal.

Biosensor research has been on a steep upward trajectory due to the ongoing requirements for low-cost, rapid and sensitive detection systems in a range of fields. From 1984 to 1997, the amount of scientific publications and patents in regards to this topic were around 6000 and 600, respectively according to the commercial report by Fuji Keizai (5,6). These numbers have seen a significant increase, along with the emerging field of nanobiotechnology. By 2004, biosensor R&D produced over 6000 articles and 1100 issued patents within only 6 years (5). Advances in biosensor technology are driven by the strong market demand. Currently, biosensing devices are not only applied in medical or biotechnological applications, but have been widely used for *in situ* monitoring in fields such as food technology, environmental monitoring, homeland security and bio- and chemical processing (7,8). However, the fastest growing sector is still the biomedical diagnostics area with a market value of $7.5 billion in 2010 which is expected to increase to $19 billion by 2020. Here, biosensors are used for disease detection (*e.g.* cancer) or disease management (*e.g.* diabetes) using specific biomarkers (9). Proteomic studies have led to the discovery of biomarkers ranging from small molecules such as fatty acids and glucose to macromolecules such as enzymes and nucleic acids (10–12). Biomarkers can be present at very low concentrations in physiological conditions. For instance, prostate-specific antigen (PSA), a biomarker for prostate cancer, has been reported to have a normal value of 23 pM (0.6 ng/ml) in serum (13,14). Therefore, in order to detect the elevation of these low-concentration biomarkers especially at the early stage of the disease, biosensors with high sensitivity and selectivity are required.

Over the past decades, the ongoing need for low-cost, simple, rapid and real-time detection systems has revolutionised the use of luminescence spectroscopy in biological analysis, monitoring and imaging (15–18). In luminescence spectroscopy, the detection is based on the luminescence intensity readings of the emitting target or analyte either directly or *via* an additional label (19). Luminescence detection paradigms have key advantages over other optical platforms such as absorbance, reflectance or interferometric based detection (19,20) (see Table I). The sensitivity of luminescence-based detection system has been reported to provide excellent limits of detection down to femto- and picomolar levels (19,21) due to the ability of this technique to quantify light emissions down to a few photons using photomultiplier tubes or photodiodes (22).

LUMINESCENCE-BASED SENSING

Photoluminescence-Based Biosensing

The term luminescence refers to the type of emission generated by the relaxing of electrons from the lowest excited state to its electronic ground state. Photoluminescence is initiated by photoexcitation, the absorption of photons supplied by an external energy source (*i.e.* light). Electrons are excited by photons from the ground to an excited state, either singlet (S_1) or triplet state (T_1). Following the excitation, the electrons relax to a ground state (S_0) releasing photons which are emitted as light (23,24). A singlet-to-singlet ($S_1 \rightarrow S_0$) emission mechanism (*i.e.* spin allowed transition) is defined as

Table I Advantages and Disadvantages of the Current Optical Detection Methods

Optical detection methods	Advantages	Disadvantages
Absorbance measurements	• Simple; as it measures the concentration difference based on the absorption wavelength of the analytes. • Fast; the measurement of one sample only takes a few seconds • Ease of use	• Low sensitivity and selectivity; due to the interference by compounds other than the analyte leading to false positive readings
Surface plasmon resonance	• Simpler, faster and minimal sample preparation • Ease of use • Signal interference by compounds other than the analyte is minimised • Higher sensitivity • Real time detection	• Low specificity due to the non-specific binding leading to false positive readings • Not suitable for detection of small molecules (MW < 1000 Da) • Requires the presence of an external incidence light
Interferometric measurements	• Simple structure • Lower cost • High sensitivity and reliability • Label-free • Potential for miniaturisation	• Non-specific to the target analytes leading to false positive readings • Requires the presence of an external incidence light
Luminescence measurements	• Highly sensitive, as the luminescence intensity is proportional to the excitation intensity, hence weak signals can be detected. • High selectivity and specificity • Suitable for the detection of small and single molecules • Real time detection	• Requires the presence of an external incidence light • For non-luminescent analytes, an external dye/label is required • In fluorescence measurements, background autofluorescence may be detected leading to false positive readings

fluorescence, while a triplet-to-singlet ($T_1 \rightarrow S_0$) emission mechanism (*i.e.* spin forbidden transition) is called phosphorescence (24). The luminescence lifetime, τ, is defined as the average relaxation time for the electrons to reach the ground state. In photoluminescence-based sensing, the changes of either the luminescence lifetime or intensity of the luminescence probes are monitored (25). The spectral properties of the probes determine the sensing conditions such as the excitation and/or emission wavelength and sensor time resolution (26). These luminescent probes are also commonly known as a fluorophore or the emitting molecule. In this review, the term fluorophore will be used to define fluorescent organic molecules, while emitting molecule will be used to describe inorganic molecules with emissive properties.

Fluorescence Reporters

Fluorophores used in biosensing can be categorised into two types: the natural or intrinsic fluorophores and the extrinsic fluorophores (26). Natural fluorophores are molecules that fluoresce due to the specific moiety in their structure. These include proteins, which consist of aromatic amino acids such as tryptophan, tyrosine and phenylalanine (27,28). The detection of tryptophan *via* fluorescence, for example, has been demonstrated using a Zn(II) complex (29). This complex incorporates two anthracene subunits in which the fluorescence of the Zn(II) complex is switched off or quenched upon reaction with tryptophan. The Zn(II) probe forms a 1:1 complex with tryptophan. The quenching is attributed a through space photoelectron process from the nitrogen atom in the secondary amine of the tryptophan subunit to the excited state of the anthracene.

Enzymes and coenzymes are generally known to be fluorescent, due to the presence of these aromatic amino acid moieties. For instance, the fluorescence of glucose oxidase enzyme (GOX) is mainly attributed to the tryptophan moiety in the UV range (~335 nm) and the flavin adenine dinucleotide coenzyme in the visible range (~520 nm) (30). GOX is commonly used for the monitoring of glucose and there is currently a commercially available fluorescence assay kit for determining the GOX activity (Sigma-Aldrich, EC 1.1.3.4). However, these kits rely on a probe which fluoresces upon reaction with hydrogen peroxide (H_2O_2), one of the products of the enzymatic reaction of glucose with GOX (31). Other fluorescent molecules which plays an important role in biological reactions are the coenzymes nicotinamide-adenine dinucleotide hydrogenase (NADH) and its phosphate form (NADPH). NADH or NADPH is a natural fluorophore owing to their reduced nicotinamide ring, with a fluorescence lifetime of 0.4 ns in aqueous buffer. The short-lived fluorescence is due to the quenching of the nicotinamide by the adenine moiety in the structure of the molecule. It has been reported that the quantum yield of NADH is increased when bound to proteins. Consequently, the fluorescence lifetime also increases. The fluorescence lifetime is extended to 5 ns when the coenzyme is bound to horse liver alcohol dehydrogenase and octopine dehydrogenase (26). The distinct difference in fluorescence between NADH and its oxidised form (NAD^+) has been established for the assay of L-lactate dehydrogenase (LDH) enzyme (12). The up-regulation of this enzyme has been correlated with cell death levels and is indicative of

various pathological conditions, such as cancer and chronic wounds (32–36). When LDH is present, it catalyses the conversion of pyruvate into L-lactate, NADH is oxidised into NAD^+ and consequently the fluorescence is attenuated. This effect allowed the release of LDH to be monitored by the decrease of the fluorescence intensity of the co-enzyme (37,38). However, the drawback of this detection system is that the low excitation wavelength at 340 nm may damage the cells when the assay is conducted *in vivo*.

An extrinsic fluorophore is used in biosensing when the target molecule is non-fluorescent. The fluorescence signal is obtained by labeling or tagging the molecules with well-known fluorescent dyes. These fluorophores exhibit longer excitation and emission wavelengths compared to aromatic amino acids. Rhodamine is one of the most widely used organic dyes and covers applications ranging from optoelectronics to biomolecular imaging (39–41). Molecules based on the dye include Rhodamine 6G and Rhodamine B, which contain a reactive functional group for efficient labeling and exhibit maximum emission at 595 nm in 0.1 M Tris buffer (pH 8.0). Derivatives of the Rhodamine dye family have been developed with improved photophysical properties such as increased fluorescence intensity and photostability (42). Those derivatives, which include recently developed Alexa 546 and 555, possess different functional groups for molecular attachment and have been applied as molecular tags in high throughput imaging (15).

In toxicology and cell viability assays, the resazurin (7-hydroxy-*3H*-phenoxazin-3-one-10-dioxide) dye and its derivatives has been commonly used as label (43). Frequently known as Alamar Blue (44), the dye is only weakly fluorescent in its pure form. The compound consists of a phenoxazine group, which contains a heterocylic N-oxide group that loses its oxygen upon reduction and forms the strongly fluorescent product, resorufin (7-hydroxy-*3H*-phenoxazin-3-one, ex/em 545 nm/583 nm). The reduction of the dye into resorufin is preceded by the acceptance of an electron from coenzymes such as NADH and NADPH. The 'resazurin reduction test' is widely applied in bacterial contamination and mammalian cell proliferation assays (44,45).

Luminescent Lanthanide Complexes

Time-gated fluorescence or phosphorescence is of interest as it offers higher sensitivity than fluorescence techniques. The phosphorescence-based detection utilises luminescent probes, such as lanthanide complexes, as the emitting molecules. Lanthanides, commonly known as the rare-earth elements, are the compounds that range from lanthanum to lutetium in the periodic table. These elements possess long luminescence lifetimes (~ms) which allows time gating of the emission, hence removal of background autofluorescence (24). Several studies have shown lanthanide complexes as luminescent probes as well as labels for the molecule of interest. The emission is measured through the long-lived fluorescence or phosphorescence. These complexes are popular as sensitive labeling reagents that permit the simultaneous analysis of multiple targets at low concentrations, due to their distinctive emission wavelengths and emission lifetimes (16).

Lanthanide ions feature a line-like emission, *i.e.* narrow emission band with sharp peaks where the half value of the emission peak is approximately 10–20 nm (46). The Stokes shift, which is the difference (in wavelength or frequency) between the absorption and emission peak, can reach more than 200 nm (46–48). Direct excitation of lanthanide ions occurs in the ultraviolet range (Eu(III) and Sm(III) 395 nm, Tb(III) and Dy(III) 373 nm) while emission is in the red (Eu(III) 615 nm, Sm(III) 642 nm), yellow (Dy(III) 572 nm) and green visible spectrum (Tb(III) 545 nm). The large Stokes shift avoids any overlap between the excitation and emission spectrum, which is often observed in organic fluorescent dyes. In biosensing, this is an important characteristic in isolating the specific emission from background autofluorescence and scattering (49). Due to the long-lived fluorescence, the lanthanides have been applied in high sensitive assay technology such as the Homogeneous Time Resolved Fluorescence (HTRF) (21,50). The HTRF assay combines the standard fluorescence resonance energy transfer (FRET) with time-resolved measurements. The energy transfer between two fluorophores, a donor (long-lived) and an acceptor (short-lived) occurs when in close proximity. The energy donor consists of a lanthanide complex in which the lanthanide ion (Eu(III) or Tb(III)) is tightly embedded in a macrocycle. When the Ln(III)-labeled antigen is present, it binds with the dye-labeled antibody. Due to the close proximity of the antigen-antibody, FRET occurs between the Ln(III) complex and the dye, hence the fluorescence of the dye is enhanced. When detecting the target antigen, the labeled antigen is displaced followed by a change in the fluorescence intensity. The advantage of the HTRF assay is that it has a time delay (50–150 μs) between the initial light excitation and fluorescence measurement (50), introducing a 'measurement window' which eliminates the short-lived background and non-specific fluorescence (Fig. 1).

Chemiluminescence-Based Biosensing

In chemiluminescence (CL), the energy for the excitation of the electrons is produced from the chemical reaction between the molecules of interest followed by non-thermal emission of light (51,52). Hence, the technique offers a more advantageous means of detection compared to photoluminescence-based sensing since it does not rely on an external energy source. The detection *via* chemiluminescence has gained much interest in *in vivo* research as the method may generate clear output signal as a result of the high signal-to-noise ratio (19,22). A chemiluminescent biosensor for dansyl-labeled

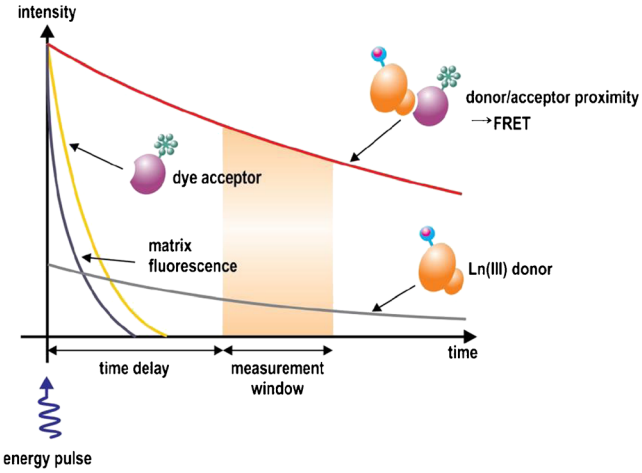

Figure 1 The fluorescence intensity *versus* time in HTRF assays. The energy pulse (from the flash lamp or laser) is followed by a time delay, allowing the elimination of the short-lived fluorescence. The graphic shows the FRET signal intensity generated at 665 nm (*red curve*), emission of Ln(III) donor at 620 nm (*grey curve*) and the fluorescent signal from acceptor dyes (*yellow curve*). (Adapted with permission from Ref. (50)).

amino acids has been reported by Lin and Yamada (53). The dansyl-l-phenylalanine (dns-l-phe) was used as a template molecule imprinted on a methacrylic acid and 2-vinylpyridine polymer. The reaction took place in a flow cell, which was filled with streams of $KHSO_5$ and Co^{2+} and the molecular imprinted polymer. The reaction between dns-l-phe and $KHSO_5/Co^{2+}$ occurred and CL was emitted. The detection limit of the CL sensor was reported to be in the range of 10^{-9}–10^{-7} M. CL spectroscopy has also currently been reviewed for its application in multiple analysis of biological matrices, such as DNA and antibody in microarrays (51).

Proof-of-concepts of CL reactions are commonly illustrated in the detection of reactive oxygen species (ROS) (54). These species are considered important in biological and chemical systems. ROS, which include hydrogen peroxide (H_2O_2), singlet oxygen ($^1O_2$) and the hydroxyl radical ($^{\cdot}OH$), remain the model analyte of choice for continuously improving the CL-based biosensing performance. This is mostly driven by the short half-life of the species and in some cases, the requirement for near infra-red (NIR) photomultiplier tube (PMT) in the CL spectrometer. For instance, the CL detection of $^1O_2$ may be observed in the visible (634 and 703 nm) and near infra-red (NIR) (~1270 nm) range, corresponding to the dimol and monomol light emissions, respectively (55). The CL emission at ~1270 nm has been reported to be more specific and non-invasive (54). In ROS detection, the weak emission generated by CL can be easily enhanced by use of reagents such as luminol (56) and lucigenin (57). These reagents have been established for amplifying the CL detection of low levels of superoxide radicals.

Another specific detection mechanism for ROS is by utilising a molecule which reacts with the ROS (*i.e.* chemical trap) forming an identified specific product. Applying a chemical trap may also amplify the intensity of the CL emission (58,59). The most common chemical traps are applied in the monitoring of $^1O_2$. These chemical traps react specifically with $^1O_2$ followed by a change in the photophysical properties of the trap. One example of a chemical trap is polycyclic aromatic hydrocarbon (60) which forms an endoperoxide upon reaction with $^1O_2$. The monitoring of $^1O_2$ is obtained through the generation of CL during the decay of endoperoxide (61). The tetrathiafulvalene (TTF) based probe, for example, offers great sensitivity for $^1O_2$ as low as 76 nM in buffer (61). However, due to the short emission lifetime of the decaying endoperoxide, the emission monitored through CL may be drowned out by background autofluorescence, particularly when the detection is performed on living cells.

Given that chemiluminescent molecules are prone to decay with a short-lived emission lifetime, more recent work has been conducted to synthesise a more stable chemiluminescent probe, which can be stored and thermally activated when required. Baumes and coworkers (62) have developed a squaraine rotaxane-based endoperoxide through irradiation of the rotaxane compound for 30 min in the presence of oxygen. The endoperoxide product was stored at −20°C as a solid or in an organic solution and was easily activated upon warming to body temperature.

The CL technique is sensitive and simple which opens new possibilities for the development of precise and miniaturised detection devices (63,64). The detection *via* CL has been demonstrated in micro- and nanostructures. For instance, the microfluidic enzyme immunoassay (μFEIA) has been investigated on silicon microchips (63). Horseradish peroxidase (HRP) was used to label the enzyme and different antibodies were immobilised on the microchips. Similar to silicon, gold nanoparticles (AuNPs) have been widely used for the initiation of solution phase CL reactions as catalysts, reducing agents, energy acceptors and nanostructured reaction platforms. (52) The detection of a cell apoptosis enzyme, caspase, through CL energy transfer (CRET) on a AuNPs has been reported to be highly sensitive with a limit of detection (LOD) as low as 20 pM (56). The system consisted of AuNPs modified with HRP. In the presence of luminol and H_2O_2, CRET occurred which resulted in the quenching of the luminol by the AuNPs. The quenched CL of luminol was easily recovered upon cleaving of the substrate by the caspase enzyme.

AN OVERVIEW OF EUROPIUM COMPLEXES

Eu(III) Luminescence Concepts

As in most lanthanides, the luminescence of Eu(III) ion is generated due to the forbidden Laporte f-f transition in the 4f shell. The 4f shell is partially filled and well shielded from its

environment by the 5 s^2 and $5p^6$ shells, therefore the orbitals are relatively insensitive to the ligand field. The shielding is responsible for the unique spectroscopic properties of the Eu(III), in particular the narrow line like luminescence and the long lifetime of the excited states (21,24). It is well known that all lanthanide ions, including Eu(III), have an extinction coefficient (ε) lower than 1 L mol^{-1} cm^{-1} (65), hence the amount of light absorbed when excited directly in the 4f transition is very limited. This disadvantage can be easily overcome by applying the *antenna-effect* or *sensitisation* process (24). The process involves incorporating a fluorophore with high molar absorbance into the coordinating complex for the Eu(III) ion. Excitation occurs *via* the fluorophore followed by an intermolecular energy transfer between the excited singlet state of the antenna (S_1) to the triplet state of the antenna (T_1) and then to the excited state of the Eu(III) ion. The energy populates the metal-centered excited state, which then subsequently emits as a photon. The luminescence of Eu(III) ion in solution usually exhibits five emission bands ($^5D_0 \rightarrow {}^7F_J, J = 0$–4). The most prominent emission line for Eu(III) ion is from the $^5D_0$ state to the $^7F_2$ ground state, which generates emission at 614 nm (21,48,65). The energy transfer process is shown in the Jablonski diagram shown in Fig. 2a.

The lanthanide coordination of the fluorophore or antenna into the Eu(III) complex may be employed in either of the two general approaches forming the europium complex, as described by Moore and coworkers (21). The first approach is through *chromophoric chelate coordination*, in which the europium complex consists of one or more organic antenna (Fig. 2b). The antenna absorbs incidents light and also forms a direct coordination with the Eu(III) ion. With this approach, both Förster and Dexter energy transfer mechanisms are likely to occur between the antenna and the Eu(III) (66,67). Numerous organic ligands have been studied and applied to form complexes with Eu(III) ions. Lis *et al.* have divided them into several groups, including the β-diketonates, aromatic carboxylic acids, pyridine, quinolone and phenanthroline derivatives, nucleic acids, and supramolecular compounds (68). However, β-diketonates seem to be the most popular and most frequently studied due to their relatively easy synthesis and excellent luminescent properties. Recent work by Milanova and coworkers have demonstrated enhanced photoluminescence behaviour of a complex with β-diketonates and a coumarin derivate, in which both ligands formed a direct coordination sphere with the Eu(III) ion (69).

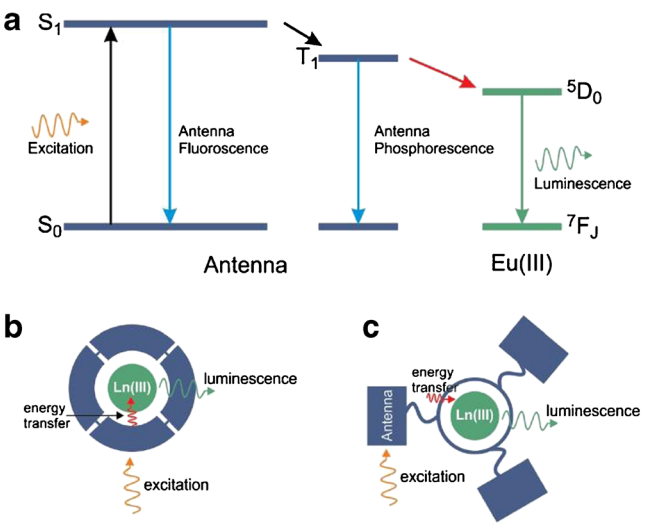

Figure 2 (**a**) Jablonski diagram of the sensitised Eu(III) by a chromophore or antenna. The illustration of the antenna effect of the Eu(III) through (**b**) chromophoric chelate and (**c**) pendant chromophore coordinations. (Adapted with permission from Ref. (21), copyright 2009 American Chemical Society).

The second approach is the so-called *pendant chromophore coordination* (Fig. 2c). In this coordination, multidentante ligands such as diethylenetriaminepentaacetic acid (DTPA) (70,71), 1,4,7,10-tetraaza-cyclotetradecane-1,4,7-triacetic acid (DO3A) (72) or 1,4,7,10-tetraazadodecane (cyclen) (73,74), bind the Eu(III) ion, forming a stable and inert complex. The antenna is linked to the complex but instead of directly coordinating the Eu(III) ion, it is covalently attached to the multidentate ligands. Hence, with this approach more organic antenna may be incorporated compared to the chromophore chelate coordination, which improves the overall absorbance and photoluminescence features of the europium complex. Given that cyclen can be easily functionalised, this ligand has become a popular core macrocyclic unit (65,75–79). Antoni *et al.* have illustrated the formation of a europium complex coordinated with cyclen functionalised with dendrimers up to the fourth generation *via* the Huisgen cycloaddition reaction (77). The ligand formed a stable linker and the triazole, as a product of the reaction, acts as an effective sensitiser in the ultraviolet region to the Eu(III) ion. Plush and Gunnlaugsson have recently developed a europium complex with a bismacrocyclic ligand (78). The ligand comprises of the core cyclen, which was tethered to a mono-aza-18-crown-ether and naphthalene fluorophore as the sensitiser. The complex was designed for the detection of small molecules such as dicarboxylic acids.

The europium ion typically has coordination numbers of eight or nine, hence the presence of an OH, NH and CH oscillator quenches the luminescence intensity and influences the lifetime of the europium complex. An ideal ligand will saturate the Eu(III) ion, as this would prevent solvent molecules, most commonly water, or an anion from binding (65). Early work by Horrocks and Sudnick have established the equation for determining the number of OH oscillators of the Eu(III) complex. This number was later referred as the inner sphere hydration number or q value (80). Parker *et al.* reviewed the determination of the q value by taking into account the OH, NH (both amide and amine) and CH oscillators in the equation (81). However, recently Supkowski

and Horrocks have established a simple equation for the q value in aqueous solution (82) using the following equation:

$$q = A_{Ln}\left[\left(\frac{1}{\tau_{H_2O}}\right) - \left(\frac{1}{\tau_{D_2O}}\right) - B_{Ln}\right] \quad (1)$$

where τ_{H2O} and τ_{D2O} are the luminescence lifetimes of the complex observed in H_2O and D_2O, respectively, while A_{Ln} and B_{Ln} are constants for a given lanthanide and solvent system in which the values are 1.1 and 1.3, respectively, for Eu(III) ion.

Application of Eu-complexes as Probes for *In-Vivo* Imaging and Small Molecules Sensing

Europium complexes have been applied for the development of contrast agents in magnetic resonance imaging (MRI) (83). Current examples of the contrast agents are the ones based on the CEST (chemical exchange saturation transfer) mechanism and the lanthanide-based agents are often referred as PARACEST agents (84–86). The CEST mechanism is more effective when applied on paramagnetic molecules compared to other CEST agents, such as DIACEST ammonia, as paramagnetic molecules displays large chemical shift (50–700 ppm) of the bound water protons or the ligand's amide or hydroxyl protons exhibiting faster exchange rates to the free water (87). The Sherry group has synthesised polymeric PARACEST agents (Fig. 3a) in which the europium complex was coordinated with cyclen having monomers on their pendant arms (85). The contrast agents were tuned for optimal CEST imaging applications. The sensitivity and the detection limits of these agents have been observed to be a function of the polymer size.

Probes based on Eu(III) complex-anthracene for the detection of $^1O_2$ have been recently reported (88–90). Recent work by Song and coworkers has developed a Eu(III)-DOTA tetraamide complex (Fig. 3b) incorporating an anthracene moiety for $^1O_2$ sensing. The complex was used as an MRI sensor for $^1O_2$ using the CEST principle (86). It was reported that the complex features advantageous properties for the MRI detection of $^1O_2$ in biological media, such as high selectivity towards $^1O_2$, rapid reaction kinetics with $^1O_2$ and water solubility. The drawback of this complex, however, is that excessive amount of the complex is required for CEST imaging in order to obtain good sensitivity.

Yuan and coworkers have also developed a luminescent Eu(III) complex-anthracene probe for *in-vivo* imaging and $^1O_2$ sensing (90). The detection principle relied on the reaction between the $^1O_2$ and the anthracene moiety, which produced a change in the luminescence intensity. The Eu(III) ion was coordinated with terpyridine, which was covalently attached with an anthracene (Eu(III)-4′-(10-methyl-9-anthryl)-2,2′:6′,2″-terpyridine-6,6″-diyl]bis(methylenenitrilo) tetrakis(acetate) or (MTTA-Eu(III)) (Fig. 4a). The probe was found to be easily transferred into living HeLa cells by incubation with a photosensitiser 5,10,15,20-tetrakis(1-methyl-4-pyridino)-porphyrintetra (toluenesulfonate) (TMPyP). The time-dependent generation of $^1O_2$ in living cells was monitored through a time-gated luminescence imaging technique in which the background fluorescence from TMPyP and cell components can be eliminated. The detection limit was reported to be 3.8 nM in carbonate buffer at pH 10.5 (90). MTTA-Eu(III) showed selectivity for $^1O_2$ giving higher phosphorescence intensity after reaction with $^1O_2$ compared to other ROS. A more recent compound developed by the same group used a different ligand to form the Eu-complex (MTDTA-Eu(III)) (Fig. 4b) (91). The detection limit was calculated at 1.3 nM, three times lower than that of MTTA-Eu(III). The neutral complex was found to be able to permeate through the cell membrane where it reacted with $^1O_2$ forming an endoperoxide that enhanced the luminescence.

The Eu(III)-tetracycline complex (Eu[tc]), a luminescent probe for hydrogen peroxide, was developed by Wolfbeis and coworkers (92,93). It was observed that upon reaction with H_2O_2, the Eu[tc] forms the highly fluorescent Eu(III)-tetracycline-H_2O_2 complex. The probe offers advantageous properties compared to other H_2O_2 fluorescent probes as it

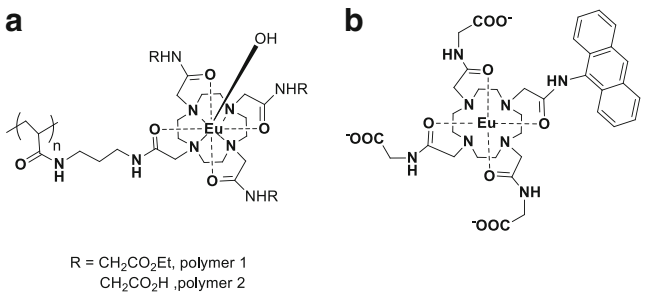

Figure 3 Structures of the Eu(III)-based PARACEST probes (**a**) Eu(III)-polyR-1,4,7,10-tetraazacyclododecane-1,4,7,10-tetraacetamide triflate salt, where polyR is either polymer 1 or polymer 2 (85), and (**b**) Eu(III)-1-N-(9-anthryl)-4,7,10,-tris-(N-acetic acid)-1,4,7,10,-tetraazacyclododecane-1,4,7,10-tetraacetamide triflate salt (86).

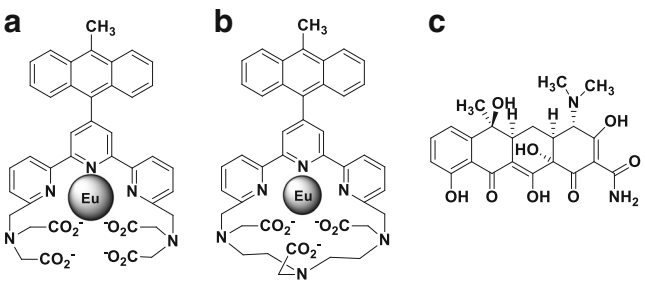

Figure 4 Structures of probes for the detection of ROS; (**a**) MTTA-Eu(III) (90) and (**b**) MTDTA-Eu(III) (91) and (**c**) tetracycline ligand for the Eu[tc] complex. (92).

works in neutral pH, has a large Stokes shift (as high as 210 nm), and a long fluorescence lifetime, which can be measured in μs. The probe can detect H_2O_2 in the range of 2–400 μM with a detection limit of 1.8 μM. In addition, the probe does not require any enzyme (such as peroxidase) or an enzyme mimic to form a fluorescent product. It was postulated that the H_2O_2 displaced the coordinated H_2O molecule in the complex without any redox reaction.

The sensing of small molecules also includes anion sensing. Monitoring anions is essential as many biological processes depend on the presence or transport of these negatively charged molecules (94). The development of anion sensors based on lanthanide ions, in particular europium, has been demonstrated by Parker and coworkers (75,95). The detection mechanism is based on the perturbation of the excited states of the europium complex due to the displacement of water molecules by anions or interactions of anions with an antenna. The europium complex (Fig. 5a), which consists of a cyclen with monoamide triphosphinate pendant arms as the coordinating ligand and a phenanthridine antenna, was synthesised as a sensor for Cl^-. The fluorescence of the phenanthridium ions is known to be quenched by halide ions. Hence, the europium complex was quenched by the addition of Cl^-, Br^- or I^- ions illustrating the good selectivity of the probe for halide ions. Since the phenanthridine antenna is also quenched by the addition of hydroxide at the 6-position forming a pseudobase, the probe was described to be sensitive to pH and hydroxide anions. Recent work by the same group developed a europium-based probe (Fig. 5b) for the citrate anion (96). The probe incorporated a new pyridothioxanthone antenna, which allows the excitation wavelength to be shifted to the red (λ_{exc} 384 nm). Upon titration with citrate, the complex showed an increased luminescence at 616 nm.

Sensing of a dicarboxylic acid such as malonic acid has been demonstrated in neutral solutions by Plush and Gunnlaugsson with a europium complex coordinated with a bismacrocyclic ligand (Fig. 5c) (78). The complex only gave an enhanced luminescence to malonic acid as opposed to other dicarboxylic acids, such as aspartic, succinic or glutaric acid due to the displacement of the O-H oscillators by strong binding to malonic acid.

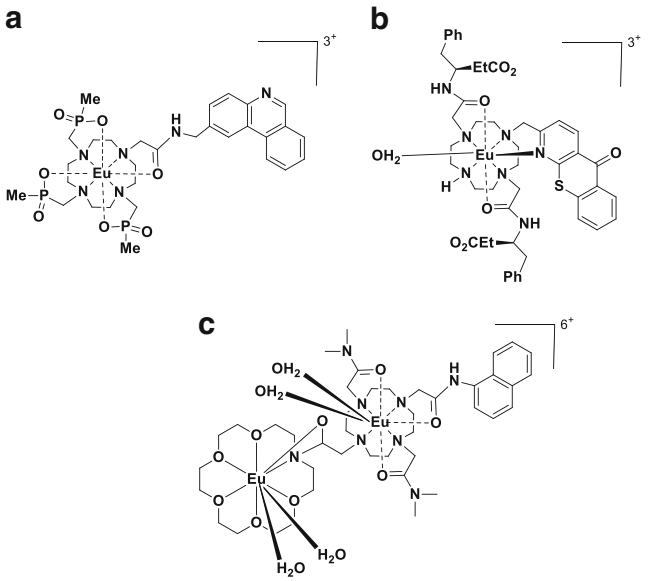

Figure 5 Structures of Eu(III) sensing probes for the detection of anions. (**a**) Eu(III)-phenanthridinum complex (75), (**b**) Eu(III)-pyridothioxanthone complex (96) and (**c**) dinuclear Eu(III) bismacrocyclic complex (78).

Application of Eu(III) Complexes for Biosensing

The excellent photoluminescence properties of the europium complex have been exploited in the detection of biological macromolecules. Recent studies have shown the application of visible emitting europium complexes as labels in ultrasensitive sensor systems with very low limits of detection (48,97). Currently, the use of Eu(III) complexes as sensitive labels is commercially available, known as the DELFIA immunoassay. The assay is based on the sensitive detection of a europium-EDTA derivative complex using time-gated fluorometry (49,98). The Eu(III) complex is conjugated to an antibody and further applied in non-competitive type (sandwich assay) or competitive type assays. When the assay is complete, the lanthanide complex is dissociated from the antibody at low pH into an 'enhancement solution' comprising of Triton X-100, *β*-diketonate and a Lewis base. This solution forms a micelle around the Eu(III) ion protecting it from being quenched in the aqueous solution. Using rabbit IgG as a model system, the sensitivity of the immunoassay was reported to be 25 pg/ml.

As opposed to the dissociation mechanism in the DELFIA assay, a non-dissociated method was introduced by Harma and coworkers in the ultrasensitive detection of a prostate cancer biomarker (97). A *β*-diketonate was used as the ligand, and the Eu(III) complex was incorporated into polystyrene nanoparticles (diameter of 107 nm). Each nanoparticle contained >30,000 Eu(III) complexes and was coated with streptavidin. The group employed a model assay system where the streptavidin-coated nanoparticles were used to trace biotinylated prostate specific antigen (PSA) in a microtiter plate. The detection limit of the biotinylated PSA was calculated at 0.38 ng/l, which corresponded to 10 fmol/l or 60 zeptomoles of PSA. The detection principle was further applied for the detection of biotinylated PSA in male serum samples, giving a detection limit of 0.83 ng/l (99).

Lu *et al.* has developed nanoparticles grafted with the Eu-EDTA-H_2O complex for the detection of an Anthrax biomarker (100). Covalent attachment of the europium complex on the nanoparticles *via* 3-aminopropyltriethoxysilane (APTES) modification provided a stable biosensor as it prevented the complex from leaching. The europium

nanoparticle was able to detect calcium dipicolinate, a biomarker for Anthrax, in aqueous solution with a response time of 2 min. The limit of detection was reported to be 0.2 nM, six orders of magnitude lower than an infectious dosage of the Anthrax spores. The grafting of Eu(III) complexes on single walled carbon nanotubes (SWNTs) through a diaminotriethylene glycol linker has also been illustrated to monitor DNA (101). DNA binding to Eu(III)-labeled SWNT resulted in an enhanced red luminescence. The luminescence intensity was reported to be a function of the DNA sequence and form, in which double stranded DNA showed the highest enhancement.

Chemiluminescence Sensing Using Eu(III) Complexes

One of the earliest CL-based sensors using a Eu(III) complex was the luminescent oxygen channeling immunoassay (LOCI). The CL detection was introduced in the mid-1990s by the group of Ullman for the detection of $^1O_2$ (102). This method relies on the short diffusion distance of the $^1O_2$ to initiate a CL reaction nearby. In this case, a particle containing a photosensitiser, generating the $^1O_2$, was placed in close proximity to a second particle containing the $^1O_2$ chemical trap (*i.e.* dioxene, thioxene and squarate dye) and the Eu(III) complex (*i.e.* $Eu(TTA)_3$phen or $Eu(TTA)_3$TOPO)). The particles were coated with the antigen or antibody of interest. When the particles are in close proximity, the $^1O_2$ generated by the first particle will diffuse to the second particle and CL occurs. The CL intensity is enhanced by the presence of the Eu(III) complexes. By using antibody coated Eu(III)-particles, the LOCI method was capable of detecting human thyroid-stimulating hormone with concentrations as low as 90 fM with a response time of 12 min. The LOCI method was reported to be three orders of magnitude more sensitive than homogenous fluorescence-based assays, such as the enzyme-linked immunosorbent assay (ELISA), owing to the absence of scattering excitation light. The LOCI method, which can be performed in microplates or applied for high throughput screening, has since been commercialised by Perkin-Elmer (103–105). Recent developments applying the LOCI technology includes detection of insulin in human plasma (LOD 0.3 pM) (106) and oligonucleotides (LOD 1 pM) (107).

Europium-based CL probes have been reported for the detection of H_2O_2 (108). The redox reaction of Eu(II)/Eu(III) was exploited for the detection of H_2O_2 in aqueous media. The study was carried out by applying europium complexes incorporating different ligands for detection. The ligand 1,4,8,11-tetraazacyclotetradecane-1,4,8,11-tetraacetic acid (TETA) was reported to have the highest CL intensity compared to other cyclic or acyclic aminopolycarboxylic acids or dicarboxylic acids ligands. This was due to the amount of nitrogen coordinating the Eu ion in the TETA ligand.

LUMINESCENCE ENHANCEMENT IN BIOSENSING

Luminescence Enhancement Concepts

Whilst luminescence-based imaging and detection techniques are considered highly sensitive for biomedical applications, these techniques rely heavily on the optical properties of the emitting molecule or fluorophore. Some of the properties include low quantum yield (*i.e.* the ratio of the number of emitted photons to the number of absorbed photons per time), low photostability and short luminescence lifetimes. In the case of organic fluorophores, most of these molecules already possess high quantum yield (~1), such as rhodamine and fluorescein. However these fluorophores suffer from photobleaching upon continuous illumination (26). The low extinction coefficient and the quenching of europium ions by water molecules can be easily overcome by designing the proper ligand and organic antenna to efficiently fulfill the Eu(III) coordination as shown in numerous studies (21,24,68,83). Nonetheless, the energy transfer of the ion or the ligand can still be perturbed by the surrounding environment (*e.g.* solvent or anions) resulting in luminescence quenching. These reasons have driven the need for the improvement of luminescence-based detection in order to lower the detection limit where single molecules can be easily monitored (109). In this context, the use of nanotechnology has gained interest in enhancing the luminescence properties of the emitting molecule.

Nanotechnology encompasses the design and engineering of materials at the atomic or molecular scale, typically having dimensions from 1 to 100 nm, creating new generations of materials such as the nanostructured porous materials and nanoparticles. These structures offer unique electrical, optic and magnetic properties that are very different compared to bulk properties (110,111). Moreover, the nanostructures have been reported to significantly improve the spectral properties of emitting molecules such as the quantum yield, photostability and luminescence lifetime.

The theory of luminescent enhancement was developed by Purcell in the 1940s and is presently known as the Purcell effect (112). The well-established theory determines that the rate of spontaneous emission depends on the electromagnetic field of the emitting substance or the fluorophore. However, it was not until three decades later an actual luminescence enhancement experiment was conducted by Drexhage (109,113). In this experiment, the radiative decay or emission rate of the emitter, a europium complex, was observed as a function of its decay time (*i.e.* lifetime) and distance from a planar metal surface, in this case a thick silver mirror (≥100 nm). Depending on the distance from the mirror, an oscillation of the reflected far-field radiation from the emitter occurred which subsequently caused a change in the lifetime of the emitter. It was observed that the lifetime was an inverse

function of the reflected field amplitude of the emitter. An increase of the Eu(III) complex lifetime was attained when the reflected field amplitude of the complex was decreased (114).

Therefore it was concluded that controlling the electromagnetic field, thus modifying the photonic mode density, requires increasing the emission rate in free space, Γ, of the emitting molecule. When the emitter is in close proximity of a surface, the rate tends to increase with an addition of the emission rate in metal, Γ_m. The quantum yield (Q_m) and the luminescence lifetime (τ_m) of the fluorophore are then calculated using Equations (2) and (3).

$$Q_m = (\Gamma + \Gamma_m) \Big/ (\Gamma + \Gamma_m + k_{nr}) \quad (2)$$

$$\tau_m = 1 \Big/ (\Gamma + \Gamma_m + k_{nr}) \quad (3)$$

where k_{nr} is the non-radiative decay rate (109). The increase in the emission rate leads to an increase of the quantum yield and a decrease in the luminescence lifetime of the fluorophore (27). The outcome of this research was the fundamental basis of what currently is known as the surface-enhanced fluorescence (SEF). SEF relies on the modification and control of the electromagnetic field surrounding the fluorophore and has been thoroughly reviewed elsewhere (23). One example of SEF includes the enhancement of the luminescent properties of a Eu(III) complex in the presence of silver (Ag) nanoparticles (115). The luminescence properties of the europium pyridine-3-5-dicarboxylic acid (PyDC) complex were investigated and an optimum enhancement factor of 3.94 was reported in the presence of Ag colloids. The enhancement reached optimum at a Ag concentration of 3.2×10^{14} particles/l, followed by a rapid decrease of the luminescence at higher Ag concentrations. The authors have reported that the overall enhancement occurs as a competitive result between the SEF and the surface plasmon resonance (SPR) of the Ag nanoparticles. The group also reported the same effect using a Eu(III)-dinicotinic acid complex. (116) As SEF is dependent on the core size and the plasmon absorbance of the metal particle, Zhang and Lakowicz demonstrated the luminescence enhancement of a dye on Ag aggregates (117). The luminescence of the phenyl-phenanthridine dye was enhanced twofold as the plasmon absorbance increased.

Due to the competition between the radiative (*i.e.* luminescence) and the non-radiative decay rate, the surrounding environment of the emitter is usually modified to maximise the radiative decay rate in order to achieve efficient luminescent enhancement. Such modification is generally known as radiative decay engineering (RDE) (114,118). In an extensive review on RDE, Lakowisz stated several factors affecting the radiative decay, which may result either in luminescence quenching or enhancement of the emitting molecule. These factors include the ability of the metal surface to absorb or scatter light. The prior resulted in the dissipation of energy causing the fluorophore to quench, while the latter generated far-field radiation leading to emission enhancement.

The dimension of the metal or surface surrounding the fluorophore is also considered as an important factor. To have a precise control over the design and preparation of certain nanostructures may lead to an increase of the fluorescence enhancement factor as shown by Pompa and coworkers (119). The group developed a novel approach to fluorescence enhancement in which ordered arrays of Au nanostructures were coupled with CdSe/ZnS nanocrystals (NC) in a polymer blend. The enhancement was achieved by coupling the spectral properties of the NC with the surface plasmon of the Au nanostructures. Fluorescent enhancement was investigated by optimising the spatial distribution and structure of the Au substrate, which consisted of nanotriangles and nanocylinders. The highest enhancement factor of 33-fold was obtained with the 100 nm wide triangular prisms. Besides the shape and size, the pattern on the metal surface also plays a role in fluorescence enhancement as illustrated by Cunningham and coworkers (120). Patterned TiO_2 on a photonic glass slab was reported to enhance the luminescence of colloidal quantum dots (QD) by a factor of 108 compared to that of an unpatterned glass slab. The reason for the enhancement was the spectral overlap between the glass slab and both the absorption and emission wavelength of the QD.

Recently, optimising the thickness of the surface substrate has also been reported to increase the SEF of an impregnated dye (121). Using porous alumina nanorods as the substrate and Rhodamine 6G as the fluorophore, it was observed that both Surface-enhanced Raman Scattering (SERS) and SEF occurred in this system. However, both mechanisms showed an inverse relationship, and by controlling the thickness of the porous alumina substrate, the SEF of the rhodamine dye could be maximised. Other work have reported that SERS can be maximised by controlling the surface feature and and the probe properties, as demonstrated by Dal Negro, *et al.* (122).

Recent Advances in Luminescence Enhancement Based Biosensing

Modification of the photonic density surrounding the emitting molecule or fluorophore, together with tuning the proximity of these molecules to the metallic particles may indeed influence the quantum yield and luminescence lifetime of the emitter. This emitter-metal interaction has since been widely applied to the sensitive recognition and detection of biomolecules (109,118).

The Lakowicz group have demonstrated emission enhancement through SEF in biotechnology applications (27). For instance, the optimisation of this particular feature has been carried out on sensing applications of dye-labeled

DNA on Ag films. (123) Enhancement on Ag films of 5 and 7-fold was obtained for Cy3-DNA and Cy5-DNA, respectively. The study found that an optimum distance of around 70–100 between the dye and the metal surface gave maximum intensity enhancement. Self-quenching of an emitter, which is one major problem in luminescence-based detection, may be reduced by placing the emitter in close proximity to a metallic surface such as an Ag island film (SIF) (124). The emission of human serum albumin labeled with fluorescein isothiocyanate (FITC-HSA) on a SIF was enhanced 17-fold compared to the emission on glass. It was suggested that the reduction of self-quenching is a result of an increase in the radiative decay when the emitter is close to a metal surface, Γ_m.

As previously stated, detection of $^1O_2$ *via* the phosphorescence of the molecule at ~1270 nm is specific and non-invasive. The quantum yield of this phosphorescence, however, is extremely small (10^{-5}–10^{-8}), resulting in a weak emission (125). Applying metal nanostructures has proven to be effective in increasing the quantum yield and amplifying the phosphorescence detection. Gold nanoparticles, for example, have been reported to give a phosphorescence enhancement of the $^1O_2$ up to a factor of several hundred. The gold nanoparticles were tuned to have the appropriate localised surface plasmons to generate an emission enhancement (126,127). Recently, SIF have also found their applications in $^1O_2$ phosphorescence enhancement using the same plasmonic principle (128). The SIFs were coated with C_{60}, a photosensitiser capable of generating $^1O_2$ with a quantum yield close to 1. The near-IR phosphorescence of $^1O_2$ was reported to be enhanced by a factor of 35.

In biosensing, nanostructures possess large surface-area-to-volume ratio (a few hundred square metres per cm^3) and produce high signal amplification which may be exploited in the context of improving the sensitivity of optical biosensors (129,130). The enhancement of CL emission through the immobilisation of chemiluminescent molecules on metal nanoparticles has recently been demonstrated. It was postulated that the electron transfer from the metal surface might facilitate the emission enhancement of CL agents such as luminol or lucigenin. Syed *et al.* demonstrated a study where luminol is functionalised on a AuNP surface (131). The luminol-labeled AuNP is capable of detecting H_2O_2 in which the signal was enhanced 5 to 10 times compared to that of solutions with the same concentration. Another study showed CL emission generated by Au nanopopcorns which were functionalised with N-(aminobutyl)-N-ethylisoluminol (132). The Au nanopopcorns are popcorn-shaped aggregation of Au nanodots which were formed through the seed growth method. This unique structure maintained its CL activity when conjugated directly to DNA or protein.

As previously mentioned, another surface enhanced spectroscopic techniques include the SERS where the Raman signal is increased dramatically when the molecules are attached to AuNP and AgNP (133,134). Katrin *et al.* have reported that the enhancement factor was 14-orders of magnitude higher than the non-resonant Raman spectroscopy, making it capable of monitoring a single molecule at biophysical ambient conditions (133). The SERS technique has been used in biophysics and biomedical applications which includes the sensitive detection of neurotransmitters (135), bacteria (136), and labeled DNA (137) with detection limits as low as 10^{-12} M. Giorgis *et al.* have demonstrated a different approach in SERS using porous silicon (pSi) impregnated in AgNPs (134). The enhancement was influenced by the pSi/Ag morphology, which can be easily tuned to match the excitation of the SPR of the nanoparticles. The system was able to enhance the luminescence of cyanine-based dyes and HRP with detection limits of 10^{-7} to 10^{-8} M.

POROUS SILICON (PSI) AS A BIOSENSING PLATFORM

The use of pSi structures received a great deal of interest in numerous applications since the accidental discovery by Uhlir in the mid-1950s (138). pSi is one of the porous materials of particular importance in the context of biosensors due to a range of its favourable material properties. The fabrication of pSi is relatively straightforward, fast and simple (7,129) compared to other porous structures such as porous alumina (139) or porous germanium (140). The pore sizes and thicknesses are easily tuned which allows the generation of multilayer pSi films with excellent photonic properties. The high surface area and the versatile surface chemistry (141,142) allows biomolecules to be covalently bound to the surface, which is important in the development of biosensors. The reflectance and photoluminescence properties enable the detection of biomolecules *via* optical reflectivity and photoluminescence, respectively (129). Most importantly, pSi is biocompatible and biodegradable, as it forms the nontoxic silicic acid ($Si(OH)_4$), making it a suitable substrate for biological applications (143–145).

Fabrication of pSi

Porous silicon is an inorganic nanostructured material that can be designed to feature aligned pores running perpendicular to the surface (146). The pores are generated by means of anodic electrochemical or photo-electrochemical etching of a silicon wafer under galvanostatic conditions in the presence of an etchant solution (7,129,147). The etching solution for the anodisation is usually composed of aqueous hydrofluoric acid (HF) as the etchant or electrolyte and a surfactant or wetting agent. Ethanol is most commonly used as a surfactant to lower the surface tension of the etching solution and allow HF to react with the silicon surface to form finer pores. A 1:1 ratio of

$HF_{(aq)}$ and ethanol solution is commonly used for electrochemical etching, although many of the recent studies have been conducted with higher HF to ethanol ratios (148,149). The reaction takes place in a Teflon cell, where the silicon wafer is positioned as the anode and a platinum wire or mesh is applied as the counter electrode. The final and stable product for Si in HF is H_2SiF_6 as shown in Equation 3, where 'h' refers to the valence band holes.

$$Si + 2h^+ + 6HF \rightarrow H_2SiF_6 + H_2 + 2H^+ \quad (4)$$

Pore formation through the anodisation process is based on the dissolution of the Si. So far, the most accepted dissolution mechanism of Si in HF associated with pSi formation are the ones proposed by Lehmann and Gösele (150). When a hole (h^+) reaches the Si surface it will cause a nucleophilic attack on a Si-H bond by a fluoride ion (F^-) and a Si-F bond is established. Due to the polarisation of that bond, another F^- attacks the Si backbonds. This is subsequently followed by the production of a H_2 molecule and electron injection into the substrate. Further polarisation induced by the Si-F groups will lower the Si-Si backbond electron density, which makes it prone to HF or H_2O attack. The Si surface atoms remain bonded to hydrogen and a silicon tetrafluoride is generated. When silicon tetrafluoride reacts with two HF molecules, the H_2SiF_6 is formed and ionised (150,151). Upon removal of a Si atom from the flat surface, an atomic size dip remains and the electric field distribution will adjust to the change in surface geometry in a way that h^+ transfers may still occur. Holes must be supplied by bulk Si in order for electrochemical pore formation to occur.

The morphology of the pores formed, such as the porosity and pore size can be adjusted by judicious choice of the etching parameters including the type of silicon wafer used, the dopant and dopant level, applied current density and the HF to surfactant ratio (147,152,153). The applied current density must be lower than the critical electropolishing current density. The thickness of the layer is solely determined by the total amount of charge used, *i.e.* at a constant current a longer etching time will result in deeper pores, producing a thicker layer (129).

The Surface Chemistry of pSi

Fresh etched pSi layers are not stable in aqueous solutions due to the nucleophilic attack on the silicon hydride-terminated surface by water, leading to oxidative hydrolysis (7). Since biosensing experiments are mostly conducted in aqueous solutions, there is a need to stabilise the pSi to maintain its photoluminescence and morphological properties. To preserve the photoluminescence property, for instance, Sailor and coworkers (154) demonstrated an oxidation method using iodine followed by oxidation in air. Since then, the formation of the Si-OH species has been accepted as the most suitable method to lower the hydrophobicity of the surface while maintaining and even improving the intrinsic luminescence properties of pSi (147,155). The formation of silanol groups has been performed either through chemical or thermal reactions.. Ozone oxidation at room temperature has been shown to form a siloxane (Si-O-Si) species on the pSi surface (144). Thermal annealing of the surface at temperatures lower than 600°C has also been demonstrated to generate the silanol groups forming a stable layer on the pSi surface (156). However, the reactivity of the surface treated by thermal oxidation is less than that of the ozone oxidation due the lower density of free silanol groups available on the surface (144).

Oxidation and generation of Si-O bonds is usually followed by a silanisation reaction. This reaction allows surface functionalisation where silanes with different terminal moieties can be tethered to the pSi surface. Silane coupling agents are commonly used to provide a stable bond between the pSi surface and an organic molecule. The silanisation reaction can significantly reduce the hydrophobicity of the pSi surface (contact angle reduced from $>99° \pm 3°$ in freshly etched pSi to $56° \pm 3°$ in silanised pSi), hence increasing its stability in aqueous solutions (157,158). Among the most commonly used organosilanes used for surface modification is APTES, which has been reported to provide an amine terminus on the pSi surface (159–161). The reaction of APTES on the oxidised pSi surface is usually performed at room temperature with a reaction time of only minutes. It is well known that the amine functional group is highly reactive and may cause polymerisation on the surface, hence mild reaction conditions are required (162–164). Other silanes with different functional groups such as isocyanate (149), chloro- (165) or iodosilanes (166) have also been reported to provide functionality to the oxidised pSi surface.

A second, common surface functionalisation method is the hydrosilylation reaction, which involves the attachment of an alkene or an alkyne on the freshly-etched Si-H surface (142). These reactions are performed at higher temperatures compared to silanisation, in an inert atmosphere to avoid moisture and oxygen which may reduce the coverage of the hydrosilylated molecules (167). This reactions yields pSi surfaces with stable Si-C bonds with different terminal functionality available, ranging from carboxylic acids, esters to alkyl halides (141,168–170) (Fig. 6).

A recent stabilisation method of pSi surface pioneered by the group of Salonen is the thermal carbonisation (TC) reaction, which is achieved by dissociation of acetylene on freshly etched pSi surfaces at high temperature (171–174). The reaction provides a thin layer of Si-C which occurs during the high-temperature annealing process (173), hence the stability of pSi in aqueous environment is greatly increased. TC can be

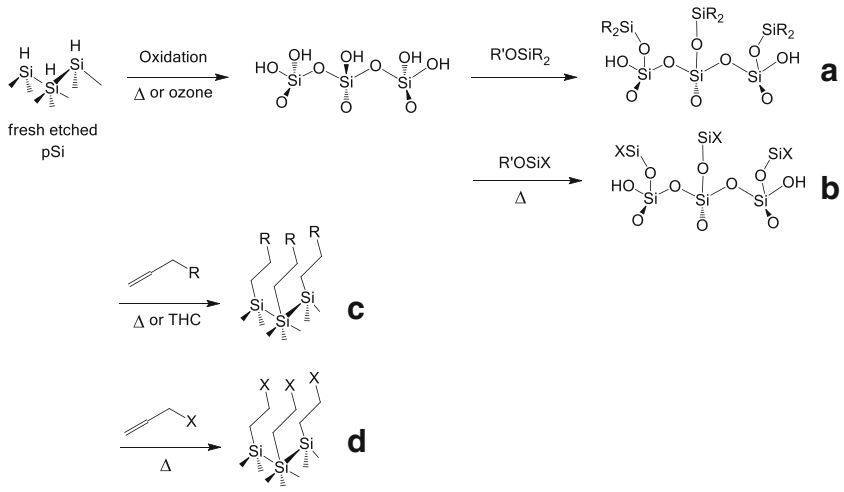

Figure 6 Fresh etched pSi undergoes oxidation which is followed by silanisation to introduce (**a**) amine groups ($R_2 = -C_3H_6NH_2$ or **b**) halide groups ($X = -C_3H_6I$). The hydrosilylation reaction was performed on the freshly-etched pSi at high temperature with or without THC to introduce (**c**) carboxylic acid groups (R = COOH) or d) alkyl halides ($X = (CH_2)_nBr$).

applied to generate either a hydrophobic or a hydrophilic pSi surface (175–178). The same group also demonstrated the thermal hydrocarbonisation (THC) method, in which the deposition of acetylene is conducted at lower temperature than TC (178,179). With the THC method, a complete surface passivation is achieved by providing a Si-CHx terminated surface, which allows further functionalisation through thermal hydrosilylation (179).

De Stefano and coworkers have also reported the use of biological films, such as hydrophobin, for surface passivation (180). Hydrophobins are protein produced by filamentous fungi (181), which self-assemble into thin, amphibilic biofilms at hydrophilic/hydrophobic interfaces. When the biofilm is bound to the silicon surface, the wettability of the pSi can be modified, protecting the nanocrystalline materials from dissolution and adding the chemical stability of pSi (180).

The pSi Microcavity

A single layer of pSi is the simplest structure generated by the electrochemical etching process, as a discrete current density is applied during the anodisation process. Changing between two different current densities (*i.e.* a high and a low current) during the etching process lead to formation of a bi-layer, hence applying multiple steps of alternating between the two current densities produces a multilayer of pSi. The current density determines the porosity and the refractive index of the pSi layer. The interchanging of high and low refractive indices produces a photonic band gap in the reflectance spectrum of the pSi multilayer called Bragg reflectors or Rugate filters when the transition between the layers are step-wise or follows a sine wave function, respectively (146).

The optical pSi resonant microcavity (pSiMC) is a 1D photonic pSi structure that is generated when a spacer layer is located between two Bragg reflectors or Rugate filters (182–184). The development of pSiMC was pioneered by Pavesi *et al.* in 1995 (185), in which the group generated the so-called dielectric Fabry-Pérot (F-P) filters. The F-P filters were obtained by inserting a spacer layer with a certain refractive index and an optical thickness of λ/2, where λ is the wavelength of the F-P transmittance, in the multilayer stack configuration. The multilayers, known as the distributed Bragg reflectors (DBR), comprised of a periodically stacked high refractive index layer (layer H) and low refractive index (layer L), each having an optical thickness of λ/4.

The reflection of white light at the surface and the bottom of a pSi layer results in an interference or fringe pattern. The F-P filter is an optical interference filter with very narrow band pass due to the multiple reflections of the parallel DBRs separated by the spacer layer (182,186), which appears as a 'dip' at the transmittance or resonance wavelength (λ) (7). The wavelength of the resonance is given by Eq. (5),

$$\lambda = n\ d \Big/ m \tag{5}$$

where n is the refractive index of the spacer, d is its thickness and m is the spectral order (182). The refractive index can be correlated to the porosity of the layer through mathematical models, such as the Maxwell-Garnett, Landau-Lifshitz-Looyenga or the widely used Bruggeman model (187,188). In the Bruggeman effective medium approximation, the pSi layer is considered as a nanocomposite of silicon and air. The nanocomposite behaves as a continuous medium and the pore sizes are much smaller than the wavelength of the incident light. (188) The porosity and the thickness of the layers can be adjusted by tuning the etching current density and time, respectively, therefore the pSiMC can be easily designed and prepared. In the etching process, the microcavity was generated by first forming the top mirror or DBR through alternating the current density of the H and L layers. The process was followed by changing the anodisation conditions to form the

spacer layer and finally the formation of the bottom mirror or DBR.

The quality of the pSiMC is determined by the energy stored within the structure or the Q factor, which follows the equation,

$$Q = \lambda / \Delta\lambda \quad (6)$$

where λ is the resonance wavelength of the pSiMC and $\Delta\lambda$ is the width of the transmittance peak also known as the full width half maximum (FWHM) of the peak (170). pSiMC with large Q-factors are a sign of small energy loss rate compared to the energy stored within the microcavity, hence more efficient light confinement (189). A high Q-factor can be obtained by increasing the porosity or the refractive index contrast between the H and L layers (185,186). In the reflectance spectrum, this can be seen as a narrow dip with FWHM less than 10 nm and DBRs with large stop bands. The position of the λ can be adjusted by simultaneously tuning the thickness of the H and L layers, as the porosities of the layers remain constant (Fig. 7). The number of repetitions of the HL layers in the DBR has also been reported to affect the position of the resonance wavelength of the pSiMC (185) as well as the reflectivity of the DBR (186). Increasing the repetition leads to increased reflectivity (~1) followed by an increased width of the stop band. In the microcavity structure, theoretically, a symmetrical breaking of the stop band of the DBR occurs when the optical thickness of the spacer layer is $\lambda/2$. However, since the top DBR has an interface with air and the bottom DBR with the bulk Si, the actual reflectance spectrum is generally asymmetrical (186).

The photoluminescence properties of pSi has intrigued researchers since the discovery of this phenomenon by Canham (190). Since its discovery, it has been accepted that the photoluminescence of pSi results from a combination of quantum confinement and the surface phenomena due to the oxide-related defects near the interfaces between Si and SiO_2 (191). In a pSi single layer, the luminescence spectrum has an FHWM value of 200 nm and the maximum of emission can vary between about 500–900 nm (147). However, in a pSiMC, the FHWM value can be narrowed down to 10 nm forming a single peak. The spacer layer is usually relatively thick (>1 μm) and an increase of thickness of the active layer influences the number and sharpness of the reflectivity dips, therefore increasing the number of photoluminescence peaks (192). At ~200 nm, one reflectivity dip is present, while at ~3.5 μm up to seven reflectivity dips are observed.

pSiMCs in Optical Biosensing

Previous studies have verified the sensitivity of pSiMCs as biosensing platforms based on reflectivity (31,193–195). The dip or the resonant wavelength in the reflectance spectrum of the pSiMC is highly sensitive to changes in the effective refractive index of the spacer layer (196). This change depends on what is attached to the pore walls and the magnitude of change is related to the density of molecules attached to the internal surface of the pSiMC (197). An in-depth study by

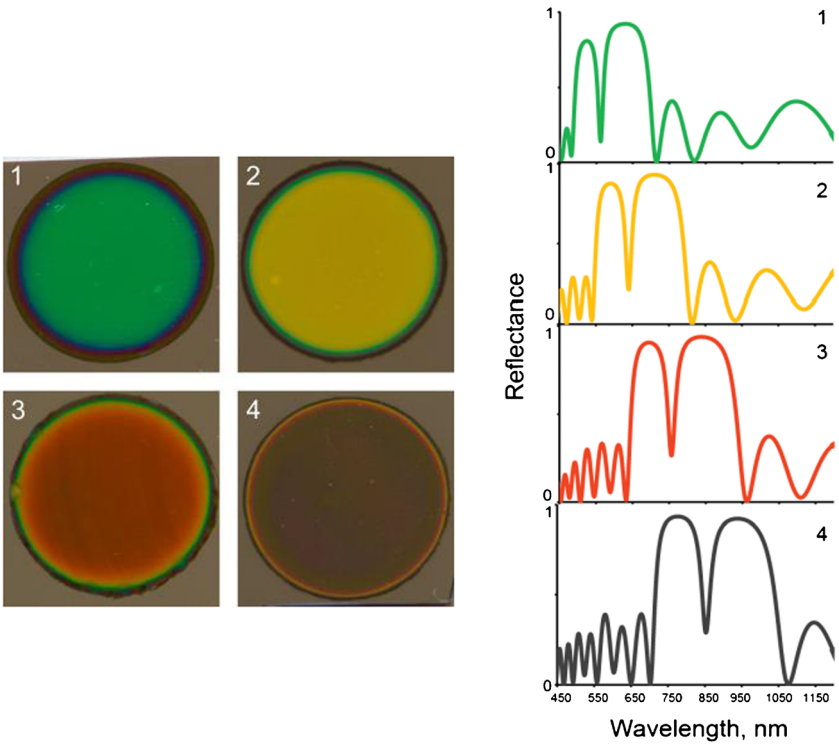

Figure 7 (**a**) Photographs of fresh etched pSiMCs designed at different resonance wavelengths (λ) and (**b**) the corresponding reflectance spectra. The pSiMCs were formed by H and L layers with porosities of 80.9% and 61.6%, respectively. The configuration of the pSiMCs were $(HL)_3$-H_4-$(LH)_3$. The thickness of each layers were adjusted accordingly to form pSiMC (1) with λ = 560 nm, pSiMC (2) with λ = 637 nm, pSiMC (3) with λ = 753 nm and pSiMC (4) with λ = 851 nm at normal incidence.

Rossi *et.al.* has demonstrated a uniform concentration distribution in a pSiMC when exposed to chemical vapours, hence time-resolved measurements of the resonance wavelength may be conducted (198). Combined with the large surface area of the pSi, the microcavity structure is therefore highly sensitive for the detection of biomolecules. A quantitative study of the sensitivity of biosensors based on pSiMC structures was performed by Ouyang *et al.* (197) They calculated the sensitivity as a function of pore size, thickness of layer binding on the pore walls and changes in refractive index using a simplified effective medium approximation.

The pSiMC structure provides a clear 'on/off' signal in its reflectance spectrum upon changes in refractive index as shown by Chan *et al.* (193) Besides clear signal output, the microcavity structures are relatively stable throughout the processing steps in development of biosensor, *i.e.* silanisation and attachment of biomolecules (192). Fauchet and coworkers prepared the pSiMC through multilayer etching where a silanisation process was performed to covalently immobilise asingle strand (ss) DNAThe attachment of DNA on the surface did not degrade the microcavity structure. Another study showed that the multilayers inside the pSiMC structure allow for the size exclusion of non-specific biomolecules and aggregates, assuring the selective penetration of non-aggregated target molecules. These molecules encounter the free active functional groups deep in the microcavity, therefore the selectivity is relatively higher within the structure than on the surface of the microcavity (31,194). Palestino *et al.* have compared the optical response of microcavities with that of pSi monolayers as well as bilayers where both of the structures also produce high optical responses due to the high quantity of the molecules attached. The absolute value of reflectivity in pSi mono- and bilayers is only ~30%, while for microcavity structures is ~100% (194). A comprehensive study by DeLouise *et al.* (130) measured the sensitivity of pSiMCs by determining the activity of glutathione-S-transferase enzyme, which showed a redshift in the optical sensor response. . It was reported that the LOD of the system ranged between 50 and 250 pg/mm^2. This work afforded a basic understanding of the dependence of the sensitivity of pSiMCs on their morphology and architecture. It was concluded that sensitivity was a function of the resonant wavelength, porosity and pore diameter. Therefore, in order to measure the sensitivity, the biomolecules need to be distributed homogenously throughout the pSiMC, which can be achieved by increasing the pore diameter, using a flow cell or designing the pSiMC to operate within the IR range.

Besides the interferometric-based biosensing, another technique has been explored with pSiMC structures. The study initiated by Wu *et al.* (199) explored the change in reflectance intensity on a fixed wavelength on a pSiMC structure and argued that this method offers higher detection sensitivity than the interferometric method by measuring the intensity change at a fixed wavelength (200). A microcavity structure was chosen since it is able to produce a narrow dip at a certain resonant wavelength in its reflectance spectrum. By using glucose as the target molecule, the pSiMC proved to be advantageous at lowering the detection limit while still achieving high reliability. Compared to the redshift interferometric method, the limit was lowered by an order of a magnitude.

pSiMCs as Luminescence Enhancers

The low reflectance of the dip in the reflectance spectrum is caused by light being trapped and absorbed in the spacer layer (182). Therefore the pSiMC is an excellent host-matrix for emitting materials, which permits the sharpening of the emission spectrum and amplification of the luminescence of the emitted material (31,201–205) (Fig. 8). For example, a Rhodamine 800 (LD800) dye incorporated inside the pSiMC has a luminescence enhancement of 80 units at 710 nm over the same dye impregnated in a pSi single layer for a certain excitation angle (203). QD have also been studied for their optical properties when confined inside an active layer of pSiMC (204,206). A study conducted by DeLouise and Ouyang has prepared pSi surfaces adsorbed with surfactant capped Cd/Se core and CdSe/ZnS core/shell QD (206). The fluorescence enhancement properties were compared between the single layer and microcavity structure. The fluorescence enhancement depended on the structures as well as the surface chemistry of the pSi. The result also indicates that the highest fluorescence enhancement of QD was observed on

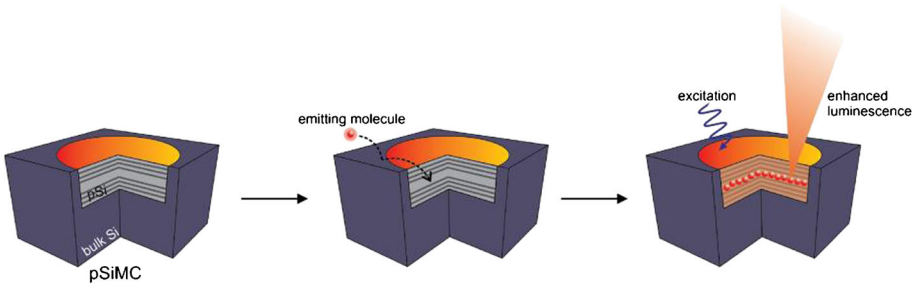

Figure 8 Schematic of pSiMC as a luminescence enhancer for the confined emitting molecule. The simplified illustration shows that upon excitation of light, the luminescence enhancement is generated from the emitting molecule confined in the spacer layer of the pSiMC.

thermally oxidised microcavity samples having a resonance tuned with the QD emission (*i.e.* 630–650 nm).

PSIMC-BASED ULTRASENSITIVE BIOSENSORS *VIA* LUMINESCENCE ENHANCEMENT

Single layers of pSi have been applied as biosensors based on photoluminescence as reported by Rossi, *et al.* (207) The biosensor was developed for the detection of dye-labeled bacteriophage virus with a detection limit as low as 2×10^7 plaque-forming units per ml (pfu/ml). However, the sensing performance could be further improved by optimising the structure of the porous layer, as stated by the authors.

Given that the pSiMC is an efficient luminescence enhancer due to its unique structure, this attribute has been exploited recently in the development of ultrasensitive biosensors (31,161,194,202,208). These biosensors focus on the manipulation of the optical density of the fluorophore or the emitter confined inside the microcavity layers. One of the early examples of pSiMCs as sensors was the one developed by Levitsky *et al.* (209) The microcavity platform was incorporated with a fluorescent polymer able to detect nitroaromatic explosives. Upon exposure to the explosive vapours, the sensor showed that the fluorescence was attenuated at the resonant wavelength of the pSiMC.

As the spacer layer of the pSiMC structure confines light and provides spontaneous emission according to the Purcell effect, the luminescence signal of a confined fluorophore is enhanced generating a biosensor with increased sensitivity. The effect of the spacer layer for signal enhancement was demonstrated by Palestino *et al.* (31) The emission of the confined fluorophores was compared between that of a pSi single layer, multi-layer and microcavity. The biotinylated structures were applied to detect the fluorescein isothiocyanate (FITC) labeled streptavidin. The result showed that the pSi microcavity demonstrated excellent fluorescence enhancements for the fluorescent protein. The authors stated that the enhancement was due to the coupling of the emission of the fluorophore and the strong optical field intensity of the spacer layer.

The fluorescence enhancement feature has also been observed on a more complex structure namely the pSi coupled microcavity (PSCM) developed by Sciacca *et.al* (202). A PSCM consists of two active layers, which are surrounded by adjacent DBRs resulting in a double resonance in the reflectance spectrum. The double resonance causes an enhancement of both the excitation and the emission of the fluorophore. Their work showed that small concentrations of labeled protein down to 10^{-9} M can be detected.

Eu(III) Complex in pSiMC and the Potential for Biosensing Applications

The energy transfer between Eu(III) and pSi structure has been reported in previous studies (210,211). Elhouichet *et al.* suggested that the Si nanocrystallites may have influenced the excitation of the Eu(III) ion resulting in improved luminescence of the lanthanide (212). The Europium Nanoparticles for Signal enhancement of Antibody Microarrays (ENSAM) applies europium-containing nanoparticles and pSi for signal enhancement in microarray assays (14). Similar to the work of Harma and coworkers (97) the europium-β-diketonate was incorporated into polystyrene nanoparticles to which streptavidin were conjugated. However, instead of using a microtiter plate, these nanoparticles were then applied for detecting biotinylated-PSA arrayed on a pSi chip. The luminescence of the ENSAM assay gave a 10-fold enhancement compared to the assay conducted with streptavidin labeled with Eu(III) complex. This was attributed to the amount of Eu(III) complex incorporated in a single nanoparticle. Moreover, due to the nanoporous structure of the pSi, the high surface area allowed more antibodies to be deposited compared to the flat Si or nonporous structures. Using the ENSAM assay, the LOD for PSA was less than 0.14 ng/ml.

Combining the excellent photophysical properties of the Eu(III) complex and the ability of the pSiMC structure to enhance the luminescence may indeed generate a highly sensitive biosensor. Recently, Voelcker and coworkers have demonstrated the luminescence enhancement of a Eu(III) complex covalently attached inside a pSiMC (170). The enhancement was a result of precise and controlled electrochemical etching, generating a microcavity with tuned porosity and thickness. The electric field inside the spacer layer reached a twofold higher value than in free space, explaining the enhancement in the rate of spontaneous emission of the Eu(III) complex. Aligning the resonance wavelength of the pSiMC with the maximum luminescence of the Eu(III) complex also contributed to the enhancement due to the Purcell effect within the microcavity (112,213). The luminescence of the Eu(III)-1,4,7,10-tetraazacyclododecane-4,7,10-triacetic acid-1-(N-(prop-2-yn-1-yl) acetamide, which has weak emission characteristic due to the absence of an antenna, was enhanced more than threefold when compared to other pSi structures without spacer layer. This feature was then further applied in the detection of Eu(III) complex labeled streptavidin on a biotinylated pSiMC surface (214). The Eu(III)-1,4,7-Tris(carbonylmethyl)-10-(4′-quinolineacetic acid, (7′-acetamide)-1′,2′-dihydro-2′-oxo)-1,4,7,10-tetraazacyclododecane incorporates the carbostyril antenna in the pendant arm. The carbostyril moiety absorbs at ~350 nm and is able to effectively populate the triplet state of the Eu(III) complex, hence increasing its luminescence (71,215). The results showed a similar luminescence enhancement factor to that without

antenna. The pSiMC sensor was able to detect steptavidin with concentration as low as 150 nM.

pSiMCs as Enzymatic Biosensors

Enzymatic biosensors are known to be highly sensitive and selective since the enzyme only reacts with a substrate or a class of substrates (216,217). When enzymatic reactions generate or quench fluorescence, the use of pSiMC as a detection platform can be employed to significantly increase the sensitivity of the biosensor and lower concentration could be detected.

Palestino *et al.* has described the detection of glucose oxidase in a pSiMC through fluorescence enhancement (194). The fluorescence was observed on the pSiMC, pSi single layer and Bragg reflector, which resulted in a fluorescence enhancement on the pSiMC surface. Recently, work by the Voelcker group has shown that pSiMCs enable the ultra-sensitive detection of matrix metalloproteinase (MMP) enzymes (208). In this work, the pSiMC was generated from an n-type Si wafer which has been reported to allow larger pore sizes of more than 120 nm (218). The recognition of MMP was achieved through the modification of the microcavity with a known MMP substrate consisting of a fluorophore and a quencher. In the presence of MMP, the MMP substrate was cleaved leaving the fluorophore moiety on the microcavity and the emission intensity was amplified. The LOD of MMP on a microcavity surface was reported to be 7.5×10^{-19} M. The same group has also demonstrated the detection of the L-lactate dehydrogenase (LDH) enzyme on a dye-modified pSiMC (219). The biosensor gave an excellent LOD of 0.08 U/ml and linear response between 0.16 and 6.5 U/ml which is in the LDH concentration range in normal as well as damaged tissues.

CONCLUSIONS

In summary, this review highlights recent developments in luminescence-based detection. The on-going need for a highly sensitive biosensor has driven current research to enhance such detection, which includes improving and manipulating the photophysical properties of the detection system. Inorganic nanostructures have been shown to produce enhanced luminescence of an emitting molecule or fluorophore by improving the luminescence lifetime and quantum yield. As a result, the signal is amplified and the sensitivity of the biosensing device is increased.

We believe that the concept of luminescence enhancement, particularly in a pSiMC, for the detection of biomolecules has potential for generating ultra-sensitive biosensors. The structure of the microcavity is advantageous compared to other pSi structures such as the pSi single layer or Bragg reflectors due to its optical resonance properties. With the ability of the pSi microcavity to store energy and increase the spontaneous emission of the confined emitter, the luminescence signal of the emitting molecule is greatly enhanced. A combination of the appropriate luminescence emitter with a pSiMC platform could result in ultralow detection limits, hence enable the monitoring of low abundance biomarkers.

ACKNOWLEDGMENTS AND DISCLOSURES

The authors would like to acknowledge the Australian Research Council Centre of Excellence in Convergent Bio-Nano Science and Technology (project number CE140100036). SNAJ would like to thank the Australian Government for the Australia Award Scholarship and acknowledge funding from the Wound Management Innovation CRC (Australia).

REFERENCES

1. Thevenot DR, Tóth K, Durst RA, Wilson GS. Electrochemical biosensors: recommended definitions and classification. Pure Appl Chem. 1999;71(12):2333.
2. Thévenot DR, Toth K, Durst RA, Wilson GS. Electrochemical biosensors: recommended definitions and classification1. Biosens Bioelectron. 2001;16(1–2):121–31.
3. McNaught AD, Wilkinson A. IUPAC. Compendium of chemical terminology, (the "Gold Book"). 2nd ed. Oxford: Blackwell Scientific Publications; 1997.
4. Ponmozhi J, Frias C, Marques T, Frazão O. Smart sensors/actuators for biomedical applications: review. Measurement. 2012;45(7):1675–88.
5. Fuji-Keizai. Biosensor market, R&D Applications & Commercial Implication: W.S. & Worldwide. Fuji-Keizai USA, Incorporated; 2004.
6. Luong JHT, Male KB, Glennon JD. Biosensor technology: technology push versus market pull. Biotechnol Adv. 2008;26(5):492–500.
7. Jane A, Dronov R, Hodges A, Voelcker NH. Porous silicon biosensors on the advance. Trends Biotechnol. 2009;27(4):230–9.
8. Perumal V, Hashim U. Advances in biosensors: principle, architecture and applications. J Appl Biomed. 2014;12(1):1–15.
9. Krishnamoorthy S. Nanostructured sensors for biomedical applications—a current perspective. Curr Opin Biotechnol. 2015;34:118–24.
10. Ray S, Reddy PJ, Choudhary S, Raghu D, Srivastava S. Emerging nanoproteomics approaches for disease biomarker detection: a current perspective. J Proteomics. 2011;74(12):2660–81.
11. Ray S, Reddy PJ, Jain R, Gollapalli K, Moiyadi A, Srivastava S. Proteomic technologies for the identification of disease biomarkers in serum: advances and challenges ahead. Proteomics. 2011;11(11):2139–61.
12. Moran JH, Schnellmann RG. A rapid β-NADH-linked fluorescence assay for lactate dehydrogenase in cellular death. J Pharmacol Toxicol Methods. 1996;36(1):41–4.
13. Lilja H, Ulmert D, Björk T, Becker C, Serio AM, Nilsson J-Å, *et al.* Long-term prediction of prostate cancer up to 25 years before

diagnosis of prostate cancer using prostate Kallikreins measured at age 44 to 50 years. J Clin Oncol. 2007;25(4):431–6.
14. Järås K, Tajudin AA, Ressine A, Soukka T, Marko-Varga G, Bjartell A, *et al.* ENSAM: europium nanoparticles for signal enhancement of antibody microarrays on nanoporous silicon. J Proteome Res. 2008;7(3):1308–14.
15. Price JH, Goodacre A, Hahn K, Hodgson L, Hunter EA, Krajewski S, *et al.* Advances in molecular labeling, high throughput imaging and machine intelligence portend powerful functional cellular biochemistry tools. J Cell Biochem. 2002;87(S39):194–210.
16. Woods M, Kovacs Z, Sherry AD. Targeted complexes of lanthanide(III) ions as therapeutic and diagnostic pharmaceuticals. J Supramol Chem. 2002;2(1–3):1–15.
17. Welsh DK, Kay SA. Bioluminescence imaging in living organisms. Curr Opin Biotechnol. 2005;16(1):73–8.
18. Licha K, Olbrich C. Optical imaging in drug discovery and diagnostic applications. Adv Drug Delivery Rev. 2005;57(8):1087–108.
19. Bosch M, Sánchez A, Rojas F, Ojeda C. Recent development in optical fiber biosensors. Sensors. 2007;7(6):797–859.
20. Monk D, Walt D. Optical fiber-based biosensors. Anal Bioanal Chem. 2004;379(7–8):931–45.
21. Moore EG, Samuel APS, Raymond KN. From antenna to assay: lessons learned in lanthanide luminescence. Acc Chem Res. 2009;42(4):542–52.
22. Mirasoli M, Michelini E. Analytical bioluminescence and chemiluminescence. Anal Bioanal Chem. 2014;406(23):5529–30.
23. Emmanuel F, Samuel G. Surface enhanced fluorescence. J Phys D: Appl Phys. 2008;41(1):013001.
24. Binnemans K. Lanthanide-based luminescent hybrid materials. Chem Rev. 2009;109(9):4283–374.
25. Ince R, Narayanaswamy R. Analysis of the performance of interferometry, surface plasmon resonance and luminescence as biosensors and chemosensors. Anal Chim Acta. 2006;569(1–2):1–20.
26. Lakowicz JR. Fluorophores—principles of fluorescence spectroscopy. US: Springer; 2006. p. 63–95.
27. Lakowicz JR, Geddes CD, Gryczynski I, Malicka JB, Gryczynski Z, Aslan K, *et al.* Advances in surface-enhanced fluorescence. J Fluoresc. 2004;14:10–28.
28. Davies MJ. Singlet oxygen-mediated damage to proteins and its consequences. Biochem Biophys Res Commun. 2003;305(3):761–70.
29. Fabbrizzi L, Licchelli M, Perotti A, Poggi A, Rabaioli G, Sacchi D, *et al.* Fluorescent molecular sensing of amino acids bearing an aromatic residue. J Chem Soc Perkin Trans. 2001;2(11):2108–13.
30. Lakowicz JR. Principles of fluorescence spectroscopy. Springer Science & Business Media; 2013.
31. Palestino G, Agarwal V, Aulombard R, Pérez EA, Gergely C. Biosensing and protein fluorescence enhancement by functionalized porous silicon devices. Langmuir. 2008;24(23):13765–71.
32. Hou J-M, Greystoke A, Lancashire L, Cummings J, Ward T, Board R, *et al.* Evaluation of circulating tumor cells and serological cell death biomarkers in small cell lung cancer patients undergoing chemotherapy. Am J Pathol. 2009;175(2):808–16.
33. Kastritis E, Kyrtsonis M-C, Hadjiharissi E, Symeonidis A, Michalis E, Repoussis P, *et al.* Validation of the International Prognostic Scoring System (IPSS) for Waldenstrom's macroglobulinemia (WM) and the importance of serum lactate dehydrogenase (LDH). Leuk Res. 2010;34(10):1340–3.
34. Ho J, de Moura MB, Lin Y, Vincent G, Thome S, Duncan LM, *et al.* Importance of glycolysis and oxidative phosphorylation in advanced melanoma. Mol Cancer. 2012;11(1):76–88.
35. James TJ, Hughes MA, Cherry GW, Taylor RP. Simple biochemical markers to assess chronic wounds. Wound Repair and Regeneration. 2000;8(4):264–9.
36. Zhao YH, Zhou M, Liu H, Ding Y, Khong HT, Yu D, *et al.* Upregulation of lactate dehydrogenase A by ErbB2 through heat shock factor 1 promotes breast cancer cell glycolysis and growth. Oncogene. 2009;28(42):3689–701.
37. Drent M, Cobben N, Henderson R, Wouters E, van Dieijen-Visser M. Usefulness of lactate dehydrogenase and its isoenzymes as indicators of lung damage or inflammation. Eur Respir J. 1996;9(8):1736–42.
38. Wang N, Huang D, Zhang J, Cheng J, Yu T, Zhang H, *et al.* Electrochemical studies on the effects of nanometer-sized tridecameric aluminum polycation on lactate dehydrogenase activity at the molecular level. J Phys Chem C. 2008;112(46):18034–8.
39. Anedda A, Carbonaro CM, Clemente F, Corpino R, Grandi S, Magistris A, *et al.* Rhodamine 6G–SiO2 hybrids: a photoluminescence study. J Non-Cryst Solids. 2005;351(21–23):1850–4.
40. Cho E-B, Volkov DO, Sokolov I. Ultrabright fluorescent silica mesoporous silica nanoparticles: control of particle size and dye loading. Adv Funct Mater. 2011;21(16):3129–35.
41. Chan J, Dodani SC, Chang CJ. Reaction-based small-molecule fluorescent probes for chemoselective bioimaging. Nat Chem. 2012;4(12):973–84.
42. Chen X, Tian X, Shin I, Yoon J. Fluorescent and luminescent probes for detection of reactive oxygen and nitrogen species. Chem Soc Rev. 2011;40(9):4783–804.
43. Dienstknecht T, Ehehalt K, Jenei-Lanzl Z, Zellner J, Müller M, Berner A, *et al.* Resazurin dye as a reliable tool for determination of cell number and viability in mesenchymal stem cell culture. Bull Exp Biol Med. 2010;150(1):157–9.
44. O'Brien J, Wilson I, Orton T, Pognan F. Investigation of the Alamar Blue (resazurin) fluorescent dye for the assessment of mammalian cell cytotoxicity. Eur J Biochem. 2000;267(17):5421–6.
45. Candeias LP, MacFarlane DPS, McWhinnie SLW, Maidwell NL, Roeschlaub CA, Sammes PG, *et al.* The catalysed NADH reduction of resazurin to resorufin. J Chem Soc Perkin Trans. 1998;2(11):2333–4.
46. Matsumoto K, Yuan J. Lanthanide Chelates as fluorescence labels for diagnostics and biotechnology. In: Sigel H, editor. Metal ions in biological systems: the lanthanides and their interrelations with biosystems. 40. CRC Press; 2003.
47. Huhtinen P, Kivelä M, Kuronen O, Hagren V, Takalo H, Tenhu H, *et al.* Synthesis, characterization, and application of Eu(III), Tb(III), Sm(III), and Dy(III) lanthanide chelate nanoparticle labels. Anal Chem. 2005;77(8):2643–8.
48. Handl HL, Gillies RJ. Lanthanide-based luminescent assays for ligand-receptor interactions. Life Sci. 2005;77(4):361–71.
49. Hemmilä I. Luminescent lanthanide chelates—a way to more sensitive diagnostic methods. J Alloys Compd. 1995;225(1–2):480–5.
50. Degorce F, Card A, Soh S, Trinquet E, Knapik GP, Xie B. HTRF: a technology tailored for drug discovery –a review of theoretical aspects and recent applications. Curr Chem Genomics. 2009;3:22–32.
51. Seidel M, Niessner R. Chemiluminescence microarrays in analytical chemistry: a critical review. Anal Bioanal Chem. 2014;406(23):5589–612.
52. Li N, Liu D, Cui H. Metal-nanoparticle-involved chemiluminescence and its applications in bioassays. Anal Bioanal Chem. 2014;406(23):5561–71.
53. Lin J-M, Yamada M. Chemiluminescent reaction of fluorescent organic compounds with KHSO5 using cobalt(II) as catalyst and its first application to molecular imprinting. Anal Chem. 2000;72(6):1148–55.

54. Lu C, Song G, Lin J-M. Reactive oxygen species and their chemiluminescence-detection methods. TrAC Trends Anal Chem. 2006;25(10):985–95.
55. Miyamoto S, Martinez GR, Medeiros MHG, Di Mascio P. Singlet molecular oxygen generated from lipid hydroperoxides by the russell mechanism: studies using 18O-labeled linoleic acid hydroperoxide and monomol light emission measurements. J Am Chem Soc. 2003;125(20):6172–9.
56. Huang X, Liang Y, Ruan L, Ren J. Chemiluminescent detection of cell apoptosis enzyme by gold nanoparticle-based resonance energy transfer assay. Anal Bioanal Chem. 2014;406(23):5677–84.
57. Spasojević I, Liochev SI, Fridovich I. Lucigenin: redox potential in aqueous media and redox cycling with O−2 production1. Arch Biochem Biophys. 2000;373(2):447–50.
58. Nardello V, Aubry J-M. Synthesis and properties of a new cationic water-soluble trap of singlet molecular oxygen. Tetrahedron Lett. 1997;38(42):7361–4.
59. Steinbeck MJ, Khan AU, Karnovsky MJ. Intracellular singlet oxygen generation by phagocytosing neutrophils in response to particles coated with a chemical trap. J Biol Chem. 1992;267(19):13425–33.
60. Aubry J-M, Pierlot C, Rigaudy J, Schmidt R. Reversible binding of oxygen to aromatic compounds. Acc Chem Res. 2003;36(9):668–75.
61. Li X, Zhang G, Ma H, Zhang D, Li J, Zhu D. 4,5-Dimethylthio-4′-[2-(9-anthryloxy)ethylthio]tetrathiafulvalene, a highly selective and sensitive chemiluminescence probe for singlet oxygen. J Am Chem Soc. 2004;126(37):11543–8.
62. Baumes JM, Gassensmith JJ, Giblin J, Lee J-J, White AG, Culligan WJ, *et al.* Storable, thermally activated, near-infrared chemiluminescent dyes and dye-stained microparticles for optical imaging. Nat Chem. 2010;2(12):1025–30.
63. Yakovleva J, Davidsson R, Lobanova A, Bengtsson M, Eremin S, Laurell T, *et al.* Microfluidic enzyme immunoassay using silicon microchip with immobilized antibodies and chemiluminescence detection. Anal Chem. 2002;74(13):2994–3004.
64. Ge L, Yu J, Ge S, Yan M. Lab-on-paper-based devices using chemiluminescence and electrogenerated chemiluminescence detection. Anal Bioanal Chem. 2014;406(23):5613–30.
65. Parker D, Williams JAG. Getting excited about lanthanide complexation chemistry. J Chem Soc Dalton Trans. 1996;18:3613–28.
66. Förster T. Excitation transfer and internal conversion. Chem Phys Lett. 1971;12(2):422–4.
67. Dexter DL. A theory of sensitized luminescence in solids. J Chem Phys. 1953;21(5):836–50.
68. Lis S, Elbanowski M, Mąkowska B, Hnatejko Z. Energy transfer in solution of lanthanide complexes. J Photochem Photobiol A. 2002;150(1–3):233–47.
69. Milanova M, Zaharieva J, Manolov I, Getzova M, Todorovsky D. Lanthanide complexes with β-diketones and coumarin derivates: synthesis, thermal behaviour, optical and pharmacological properties and immobilisation. J Rare Earths. 2010;28(Supplement 1):66–74.
70. Selvin PR, Jancarik J, Li M, Hung L-W. Crystal structure and spectroscopic characterization of a luminescent europium chelate. Inorg Chem. 1996;35(3):700–5.
71. Ge P, Selvin PR. Carbostyril derivatives as antenna molecules for luminescent lanthanide chelates. Bioconjug Chem. 2004;15(5):1088–94.
72. Du Z, Borlace GN, Brooks RD, Butler RN, Brooks DA, Plush SE. Synthesis and characterisation of folic acid based lanthanide ion probes. Inorg Chim Acta. 2014;410:11–9.
73. Plush SE, Lincoln SF, Wainwright KP. Fluorescent ligands derived from 2-(9-anthrylmethylamino)ethyl-appended cyclen for use in metal ion activated molecular receptors. Inorg Chim Acta. 2009;362(9):3097–103.
74. Plush SE, Clear NA, Leonard JP, Fanning A-M, Gunnlaugsson T. The effect on the lanthanide luminescence of structurally simple Eu(iii) cyclen complexes upon deprotonation of metal bound water molecules and amide based pendant arms. Dalton Trans. 2010;39(15):3644–52.
75. Parker D, Senanayake K, Gareth Williams JA. Luminescent chemosensors for pH, halide and hydroxide ions based on kinetically stable, macrocyclic europium-phenanthridinium conjugates. Chem Commun. 1997;18:1777–8.
76. Bradbury AJ, Lincoln SF, Wainwright KP. Fluorescent signaling provides deeper insight into aromatic anion uptake by metal-ion activated molecular receptors. New J Chem. 2008;32(9):1500–8.
77. Antoni P, Malkoch M, Vamvounis G, Nystrom D, Nystrom A, Lindgren M, *et al.* Europium confined cyclen dendrimers with photophysically active triazoles. J Mater Chem. 2008;18(22):2545–54.
78. Plush SE, Gunnlaugsson T. Luminescent sensing of dicarboxylates in water by a bismacrocyclic dinuclear Eu(III) conjugate. Org Lett. 2007;9(10):1919–22.
79. McCoy CP, Stomeo F, Plush SE, Gunnlaugsson T. Soft matter pH sensing: from luminescent lanthanide ph switches in solution to sensing in hydrogels. Chem Mater. 2006;18(18):4336–43.
80. Horrocks WD, Sudnick DR. Lanthanide ion probes of structure in biology. Laser-induced luminescence decay constants provide a direct measure of the number of metal-coordinated water molecules. J Am Chem Soc. 1979;101(2):334–40.
81. Beeby A, Clarkson IM, Dickins RS, Faulkner S, Parker D, Royle L, *et al.* Non-radiative deactivation of the excited states of europium, terbium and ytterbium complexes by proximate energy-matched OH, NH and CH oscillators: an improved luminescence method for establishing solution hydration states. J Chem Soc Perkin Trans. 1999;2(3):493–504.
82. Supkowski RM, Horrocks Jr WD. On the determination of the number of water molecules, q, coordinated to europium(III) ions in solution from luminescence decay lifetimes. Inorg Chim Acta. 2002;340:44–8.
83. Pandya S, Yu J, Parker D. Engineering emissive europium and terbium complexes for molecular imaging and sensing. Dalton Trans. 2006;23:2757–66.
84. Woods M, Woessner DE, Sherry AD. Paramagnetic lanthanide complexes as PARACEST agents for medical imaging. Chem Soc Rev. 2006;35(6):500–11.
85. Wu Y, Zhou Y, Ouari O, Woods M, Zhao P, Soesbe TC, *et al.* Polymeric PARACEST agents for enhancing MRI contrast sensitivity. J Am Chem Soc. 2008;130(42):13854–5.
86. Song B, Wu Y, Yu M, Zhao P, Zhou C, Kiefer GE, *et al.* A europium(iii)-based PARACEST agent for sensing singlet oxygen by MRI. Dalton Trans. 2013;42(22):8066–9.
87. Vinogradov E, Sherry AD, Lenkinski RE. CEST: from basic principles to applications, challenges and opportunities. J Magn Reson. 2013;229:155–72.
88. Song B, Wang G, Tan M, Yuan J. Synthesis and time-resolved fluorimetric application of a europium chelate-based phosphorescence probe specific for singlet oxygen. New J Chem. 2005;29(11):1431–8.
89. Song B, Wang G, Yuan J. A new europium chelate-based phosphorescence probe specific for singlet oxygen. Chem Commun. 2005;28:3553–5.
90. Song B, Wang G, Tan M, Yuan J. A europium(III) complex as an efficient singlet oxygen luminescence probe. J Am Chem Soc. 2006;128(41):13442–50.
91. Dai Z, Tian L, Xiao Y, Ye Z, Zhang R, Yuan J. A cell-membrane-permeable europium complex as an efficient luminescent probe for singlet oxygen. J Mater Chem B. 2013;1(7):924–7.

92. Wolfbeis OS, Dürkop A, Wu M, Lin Z. A europium-ion-based luminescent sensing probe for hydrogen peroxide. Angew Chem Int Ed. 2002;41(23):4495–8.
93. Wu M, Lin Z, Dürkop A, Wolfbeis O. Time-resolved enzymatic determination of glucose using a fluorescent europium probe for hydrogen peroxide. Anal Bioanal Chem. 2004;380(4):619–26.
94. dos Santos CMG, Harte AJ, Quinn SJ, Gunnlaugsson T. Recent developments in the field of supramolecular lanthanide luminescent sensors and self-assemblies. Coord Chem Rev. 2008;252(23–24):2512–27.
95. Parker D. Luminescent lanthanide sensors for pH, pO2 and selected anions. Coord Chem Rev. 2000;205(1):109–30.
96. Parker D, Yu J. A pH-insensitive, ratiometric chemosensor for citrate using europium luminescence. Chem Commun. 2005;25:3141–3.
97. Harma H, Soukka T, Lovgren T. Europium nanoparticles and time-resolved fluorescence for ultrasensitive detection of prostate-specific antigen. Clin Chem. 2001;47(3):561–8.
98. Hemmilä I, Dakubu S, Mukkala V-M, Siitari H, Lövgren T. Europium as a label in time-resolved immunofluorometric assays. Anal Biochem. 1984;137(2):335–43.
99. Huhtinen P, Soukka T, Lövgren T, Härmä H. Immunoassay of total prostate-specific antigen using europium(III) nanoparticle labels and streptavidin–biotin technology. J Immunol Methods. 2004;294(1–2):111–22.
100. Ai K, Zhang B, Lu L. Europium-based fluorescence nanoparticle sensor for rapid and ultrasensitive detection of an anthrax biomarker. Angew Chem. 2009;121(2):310–4.
101. Zhao C, Song Y, Qu K, Ren J, Qu X. Luminescent rare-earth complex covalently modified single-walled carbon nanotubes: design, synthesis, and DNA sequence-dependent red luminescence enhancement. Chem Mater. 2010;22(20):5718–24.
102. Luminescent oxygen channeling immunoassay: measurement of particle binding kinetics by chemiluminescence. 1994.
103. Singh S, Ullman EF, inventors; Google Patents, assignee. Metal chelate containing compositions for use in chemiluminescent assays. US patent 6,180,354. 2001.
104. Ullman EF, Kirakossian H, Pease JS, Daniloff Y, Wagner DB, inventors; Google Patents, assignee. Mixture of suspendable particles, one type is chemiluminescent compound capable of reacting with singlet oxygen, the other type is photosensitizer which is capable of activating oxygen to its singlet state. US patent 6,251,581. 2001.
105. Singh S, Ullman EF, inventors; Google Patents, assignee. Chemiluminescent compositions for use in detection of multiple analytes. US patent 6,406,667. 2002.
106. Poulsen F, Jensen KB. A luminescent oxygen channeling immunoassay for the determination of insulin in human plasma. J Biomol Screening. 2007.
107. Dafforn A, Kirakossian H, Lao K. Miniaturization of the luminescent oxygen channeling immunoassay (LOCITM) for use in multiplex array formats and other biochips. Clin Chem. 2000;46(9):1495–7.
108. Kaczmarek M, Staninski K, Elbanowski M. The influence of the donor atom on the chemiluminescence of Eu(III) ions in the system Eu(II)/(III)-Ligand-H2O2. Monatsh Chem. 1999;130(12):1443–51.
109. Aslan K, Gryczynski I, Malicka J, Matveeva E, Lakowicz JR, Geddes CD. Metal-enhanced fluorescence: an emerging tool in biotechnology. Curr Opin Biotechnol. 2005;16(1):55–62.
110. Jianrong C, Yuqing M, Nongyue H, Xiaohua W, Sijiao L. Nanotechnology and biosensors. Biotechnol Adv. 2004;22(7):505–18.
111. Reshetilov AN, Bezborodov AM. Nanobiotechnology and biosensor research. Appl Biochem Microbiol. 2008;44(1):1–5.
112. Purcell EM. Spontaneous emission probabilities at radio frequencies. Phys Rev. 1946;69(11–12):681.
113. Drexhage KH. IV inveraction of light with monomolecular dye lasers. Prog Opt. 1974;12:163–232.
114. Lakowicz JR. Radiative decay engineering 5: metal-enhanced fluorescence and plasmon emission. Anal Biochem. 2005;337(2):171–94.
115. Nabika H, Deki S. Surface-enhanced luminescence from Eu3+ complex nearby Ag colloids. Eur Phys J D. 2003;24(1):369–72.
116. Nabika H, Deki S. Enhancing and quenching functions of silver nanoparticles on the luminescent properties of europium complex in the solution phase. J Phys Chem B. 2003;107(35):9161–4.
117. Zhang J, Lakowicz JR. Enhanced luminescence of Phenylphenanthridine dye on aggregated small silver nanoparticles. J Phys Chem B. 2005;109(18):8701–6.
118. Lakowicz RJ, Joanna M, Ignacy G, Zygmunt G, Chris DG. Radiative decay engineering: the role of photonic mode density in biotechnology. J Phys D: Appl Phys. 2003;36(14):R240.
119. Pompa PP, Martiradonna L, Torre AD, Sala FD, Manna L, De Vittorio M, *et al.* Metal-enhanced fluorescence of colloidal nanocrystals with nanoscale control. Nat Nano. 2006;1(2):126–30.
120. Ganesh N, Zhang W, Mathias PC, Chow E, Soares JANT, Malyarchuk V, *et al.* Enhanced fluorescence emission from quantum dots on a photonic crystal surface. Nat Nano. 2007;2(8):515–20.
121. Damm S, Lordan F, Murphy A, McMillen M, Pollard R, Rice J. Application of AAO matrix in aligned gold nanorod array substrates for surface-enhanced fluorescence and raman scattering. Plasmonics. 2014;9(6):1371–6.
122. Gopinath A, Boriskina SV, Reinhard BM, Negro LD. Deterministic aperiodic arrays of metal nanoparticles for surface-enhanced Raman scattering (SERS). Opt Express. 2009;17(5):3741–53.
123. Malicka J, Gryczynski I, Fang J, Lakowicz JR. Fluorescence spectral properties of cyanine dye-labeled DNA oligomers on surfaces coated with silver particles. Anal Biochem. 2003;317(2):136–46.
124. Lakowicz JR, Malicka J, D'Auria S, Gryczynski I. Release of the self-quenching of fluorescence near silver metallic surfaces. Anal Biochem. 2003;320(1):13–20.
125. Schweitzer C, Schmidt R. Physical mechanisms of generation and deactivation of singlet oxygen. Chem Rev. 2003;103(5):1685–758.
126. Toftegaard R, Arnbjerg J, Daasbjerg K, Ogilby PR, Dmitriev A, Sutherland DS, *et al.* Metal-enhanced 1270 nm singlet oxygen phosphorescence. Angew Chem. 2008;120(32):6114–6.
127. Toftegaard R, Arnbjerg J, Cong H, Agheli H, Sutherland Duncan S, Ogilby PR. Metal nanoparticle-enhanced radiative transitions: giving singlet oxygen emission a boost. Pure Appl Chem. 2011;83(4):885.
128. Ragàs X, Gallardo A, Zhang Y, Massad W, Geddes CD, Nonell S. Singlet oxygen phosphorescence enhancement by silver islands films. J Phys Chem C. 2011;115(33):16275–81.
129. Sailor MJ, Wu EC. Photoluminescence-based sensing with porous silicon films, microparticles, and nanoparticles. Adv Funct Mater. 2009;19(20):3195–208.
130. DeLouise LA, Kou PM, Miller BL. Cross-correlation of optical microcavity biosensor response with immobilized enzyme activity. insights into biosensor sensitivity. Anal Chem. 2005;77(10):3222–30.
131. Syed LU, Swisher LZ, Huff H, Rochford C, Wang F, Liu J, *et al.* Luminol-labeled gold nanoparticles for ultrasensitive chemiluminescence-based chemical analyses. Analyst. 2013;138(19):5600–9.
132. Zhang H, Liu M, Huang G, Yu Y, Shen W, Cui H. Highly chemiluminescent gold nanopopcorns functionalized by N-(aminobutyl)-N-(ethylisoluminol) with lipoic acid as a co-stabilizing reagent. J Mater Chem B. 2013;1(7):970–7.

133. Katrin K, Harald K, Irving I, Ramachandra RD, Michael SF. Surface-enhanced Raman scattering and biophysics. J Phys Condens Matter. 2002;14(18):R597.
134. Giorgis F, Descrovi E, Chiodoni A, Froner E, Scarpa M, Venturello A, *et al.* Porous silicon as efficient surface enhanced Raman scattering (SERS) substrate. Appl Surf Sci. 2008;254(22):7494–7.
135. O'Neal DP, Motamedi M, Chen J, Cote GL, editors. Surface-enhanced Raman spectroscopy for the near real-time diagnosis of brain trauma in rats. Biomedical Spectroscopy: vibrational spectroscopy and other novel techniques; 2000 2000.
136. Efrima S, Bronk BV. Silver colloids impregnating or coating bacteria. J Phys Chem B. 1998;102(31):5947–50.
137. Graham D, Mallinder BJ, Smith WE. Detection and identification of labeled DNA by surface enhanced resonance Raman scattering. Biopolymers. 2000;57(2):85–91.
138. Uhlir A. Electrolytic shaping of germanium and silicon. Bell Syst Tech J. 1956;35.
139. Md Jani AM, Losic D, Voelcker NH. Nanoporous anodic aluminium oxide: advances in surface engineering and emerging applications. Prog Mater Sci. 2013;58(5):636–704.
140. Choi HC, Buriak JM. Preparation and functionalization of hydride terminated porous germanium. Chem Commun. 2000;17:1669–70.
141. Stewart MP, Buriak JM. Chemical and biological applications of porous silicon technology. Adv Mater. 2000;12(12):859–69.
142. Boukherroub R, Morin S, Wayner DDM, Bensebaa F, Sproule GI, Baribeau JM, *et al.* Ideal passivation of luminescent porous silicon by thermal, noncatalytic reaction with alkenes and aldehydes†. Chem Mater. 2001;13(6):2002–11.
143. Lin VS-Y, Motesharei K, Dancil K-PS, Sailor MJ, Ghadiri MR. A porous silicon-based optical interferometric biosensor. Science. 1997;278(5339):840–3.
144. Janshoff A, Dancil K-PS, Steinem C, Greiner DP, Lin VSY, Gurtner C, *et al.* Macroporous p-Type silicon Fabry−Perot layers. Fabrication, characterization, and applications in biosensing. J Am Chem Soc. 1998;120(46):12108–16.
145. Low SP, Voelcker NH, Canham LT, Williams KA. The biocompatibility of porous silicon in tissues of the eye. Biomaterials. 2009;30(15):2873–80.
146. Zhao Y, Zhao X, Gu Z. Photonic crystals in bioassays. Adv Funct Mater. 2010;20(18):2970–88.
147. Sailor MJ, Heinrich JL, Lauerhaas JM. Luminescent porous silicon: synthesis, chemistry, and applications. In: Prashant VK, Dan M, editors. Studies in Surface Science and Catalysis. 103: Elsevier; 1997. p. 209–35.
148. Schwartz MP, Cunin F, Cheung RW, Sailor MJ. Chemical modification of silicon surfaces for biological applications. Phys Status Solidi A. 2005;202(8):1380–4.
149. Szili EJ, Jane A, Low SP, Sweetman M, Macardle P, Kumar S, *et al.* Interferometric porous silicon transducers using an enzymatically amplified optical signal. Sens Actuators, B. 2011;160(1):341–8.
150. Lehmann V, Gosele U. Porous silicon formation: a quantum wire effect. Appl Phys Lett. 1991;58(8):856–8.
151. Bisi O, Ossicini S, Pavesi L. Porous silicon: a quantum sponge structure for silicon based optoelectronics. Surf Sci Rep. 2000;38(1–3):1–126.
152. Föll H, Christophersen M, Carstensen J, Hasse G. Formation and application of porous silicon. Mater Sci Eng R. 2002;39(4):93–141.
153. Salonen J, Lehto V-P. Fabrication and chemical surface modification of mesoporous silicon for biomedical applications. Chem Eng J. 2008;137(1):162–72.
154. Lauerhaas JM, Sailor MJ. Chemical modification of the photoluminescence quenching of porous silicon. Science. 1993;261(5128):1567–8.
155. Song JH, Sailor MJ. Chemical modification of crystalline porous silicon surfaces. Comments Inorg Chem. 1999;21(1–3):69–84.
156. Tsybeskov L, Fauchet PM. Correlation between photoluminescence and surface species in porous silicon: Low?temperature annealing: AIP; 1994. 1983–5 p.
157. Li H-L, Fu A-P, Xu D-S, Guo, Gui L-L, Tang Y-Q. In situ silanization reaction on the surface of freshly prepared porous silicon. Langmuir. 2002;18(8):3198–202.
158. Low SP, Williams KA, Canham LT, Voelcker NH. Evaluation of mammalian cell adhesion on surface-modified porous silicon. Biomaterials. 2006;27(26):4538–46.
159. Aissaoui N, Bergaoui L, Landoulsi J, Lambert J-F, Boujday S. Silane layers on silicon surfaces: mechanism of interaction, stability, and influence on protein adsorption. Langmuir. 2011;28(1):656–65.
160. Sweetman MJ, Shearer CJ, Shapter JG, Voelcker NH. Dual silane surface functionalization for the selective attachment of human neuronal cells to porous silicon. Langmuir. 2011;27(15):9497–503.
161. Priano G, Acquaroli LN, Lasave LC, Battaglini F, Arce RD, Koropecki RR. Rationally designed porous silicon as platform for optical biosensors. Thin Solid Films. 2012;520(20):6434–9.
162. Chiang C-H, Ishida H, Koenig JL. The structure of γ-aminopropyltriethoxysilane on glass surfaces. J Colloid Interface Sci. 1980;74(2):396–404.
163. Kim J, Seidler P, Wan LS, Fill C. Formation, structure, and reactivity of amino-terminated organic films on silicon substrates. J Colloid Interface Sci. 2009;329(1):114–9.
164. Lapin NA, Chabal YJ. Infrared characterization of biotinylated silicon oxide surfaces, surface stability, and specific attachment of streptavidin. J Phys Chem B. 2009;113(25):8776–83.
165. Jal PK, Patel S, Mishra BK. Chemical modification of silica surface by immobilization of functional groups for extractive concentration of metal ions. Talanta. 2004;62(5):1005–28.
166. Alauzun J, Mehdi A, Reye C, Corriu R. Direct synthesis of ordered mesoporous silica containing iodopropyl groups. A useful function for chemical modifications. New J Chem. 2007;31(6):911–5.
167. Böcking T, Kilian KA, Gaus K, Gooding JJ. Modifying porous silicon with self-assembled monolayers for biomedical applications: the influence of surface coverage on stability and biomolecule coupling. Adv Funct Mater. 2008;18(23):3827–33.
168. Boukherroub R, Wojtyk JTC, Wayner DDM, Lockwood DJ. Thermal hydrosilylation of undecylenic acid with porous silicon. J Electrochem Soc. 2002;149(2):H59–63.
169. Buriak JM. Organometallic chemistry on silicon and germanium surfaces. Chem Rev. 2002;102(5):1271–308.
170. Jenie SNA, Pace S, Sciacca B, Brooks RD, Plush SE, Voelcker NH. Lanthanide luminescence enhancements in porous silicon resonant microcavities. ACS Appl Mater Interfaces. 2014;6(15):12012–21.
171. Salonen J, Lehto VP, Björkqvist M, Laine E, Niinistö L. Studies of thermally-carbonized porous silicon surfaces. Phys Status Solidi A. 2000;182(1):123–6.
172. Sciacca B, Alvarez SD, Geobaldo F, Sailor MJ. Bioconjugate functionalization of thermally carbonized porous silicon using a radical coupling reaction. Dalton Trans. 2010;39(45):10847–53.
173. Salonen J, Laine E, Niinisto L. Thermal carbonization of porous silicon surface by acetylene. J Appl Phys. 2002;91(1):456–61.
174. Salonen J, Björkqvist M, Laine E, Niinistö L. Stabilization of porous silicon surface by thermal decomposition of acetylene. Appl Surf Sci. 2004;225(1–4):389–94.
175. Björkqvist M, Salonen J, Paski J, Laine E. Characterization of thermally carbonized porous silicon humidity sensor. Sens Actuators, A. 2004;112(2–3):244–7.

176. Salonen J, Tuura J, Björkqvist M, Lehto VP. Sub-ppm trace moisture detection with a simple thermally carbonized porous silicon sensor. Sens Actuators, B. 2006;114(1):423–6.
177. Tuura J, Björkqvist M, Salonen J, Lehto V-P. Electrically isolated thermally carbonized porous silicon layer for humidity sensing purposes. Sens Actuators, B. 2008;131(2):627–32.
178. Jalkanen T, Mäkilä E, Suzuki YI, Urata T, Fukami K, Sakka T, *et al.* Studies on chemical modification of porous silicon-based graded-index optical microcavities for improved stability under alkaline conditions. Adv Funct Mater. 2012;22(18):3890–8.
179. Jalkanen T, Mäkilä E, Sakka T, Salonen J, Ogata Y. Thermally promoted addition of undecylenic acid on thermally hydrocarbonized porous silicon optical reflectors. Nanoscale Res Lett. 2012;7(1):1–6.
180. De Stefano L, Rea I, Giardina P, Armenante A, Rendina I. Protein-modified porous silicon nanostructures. Adv Mater. 2008;20(8):1529–33.
181. Linder MB. Hydrophobins: proteins that self assemble at interfaces. Curr Opin Colloid Interface Sci. 2009;14(5):356–63.
182. Pavesi L, Mulloni V. All porous silicon microcavities: growth and physics. J Lumin. 1998;80(1–4):43–52.
183. Ghulinyan M, Oton CJ, Bonetti G, Gaburro Z, Pavesi L. Free-standing porous silicon single and multiple optical cavities. J Appl Phys. 2003;93(12):9724–9.
184. Lorenzo E, Oton CJ, Capuj NE, Ghulinyan M, Navarro-Urrios D, Gaburro Z, *et al.* Fabrication and optimization of rugate filters based on porous silicon. Phys Status Solidi C. 2005;2(9):3227–31.
185. Mazzoleni C, Pavesi L. Application to optical components of dielectric porous silicon multilayers. Appl Phys Lett. 1995;67(20):2983–5.
186. Pavesi L. Porous silicon dielectric multilayers and microcavities. Riv Nuovo Cim. 1997;20(10):1–76.
187. Theiß W. Optical properties of porous silicon. Surf Sci Rep. 1997;29(3–4):91–192.
188. De Stefano L, Moretti L, Rendina I, Rossi AM. Porous silicon microcavities for optical hydrocarbons detection. Sensors Actuators A. 2003;104(2):179–82.
189. Ouyang H, Fauchet PM, editors. Biosensing using porous silicon photonic bandgap structures. Proceeding SPIE 6005, photonic crystals and photonic crystal fibers for sensing applications. 2005.
190. Canham LT. Silicon quantum wire array fabrication by electrochemical and chemical dissolution of wafers. Appl Phys Lett. 1990;57(10):1046–8.
191. Saar A. Photoluminescence from silicon nanostructures: the mutual role of quantum confinement and surface chemistry. J Nanophotonics. 2009;3:032501.
192. Chan S, Li Y, Rothberg LJ, Miller BL, Fauchet PM. Nanoscale silicon microcavities for biosensing. Mater Sci Eng, C. 2001;15(1–2):277–82.
193. Chan S, Fauchet PM, Li Y, Rothberg LJ, Miller BL. Porous silicon microcavities for biosensing applications. Phys Status Solidi A. 2000;182(1):541–6.
194. Palestino G, Martin M, Agarwal V, Legros R, Cloitre T, Zimányi L, *et al.* Detection and light enhancement of glucose oxidase adsorbed on porous silicon microcavities. Phys Status Solidi C. 2009;6(7):1624–8.
195. Estephan E, Saab M-B, Agarwal V, Cuisinier FJG, Larroque C, Gergely C. Peptides for the Biofunctionalization of Silicon for Use in Optical Sensing with Porous Silicon Microcavities. Adv Funct Mater. 2011;21(11):2003–11.
196. Weiss SM, Fauchet PM. Electrically tunable porous silicon active mirrors. Phys Status Solidi A. 2003;197(2):556–60.
197. Ouyang H, Striemer CC, Fauchet PM. Quantitative analysis of the sensitivity of porous silicon optical biosensors. Appl Phys Lett. 2006;88(16):163108.
198. De Stefano L, Moretti L, Rendina I, Rossi AM. Time-resolved sensing of chemical species in porous silicon optical microcavity. Sens Actuators, B. 2004;100(1–2):168–72.
199. Wu C, Rong G, Xu J, Pan S, Zhu Y. Physical analysis of the response properties of porous silicon microcavity biosensor. Phys E. 2012;44:1787–91.
200. Jin L, Li M, He J-J. Optical waveguide double-ring sensor using intensity interrogation with a low-cost broadband source. Opt Lett. 2011;36(7):1128–30.
201. Setzu S, Ferrand P, Romestain R. Optical properties of multilayered porous silicon. Mater Sci Eng B. 2000;69–70:34–42.
202. Sciacca B, Frascella F, Venturello A, Rivolo P, Descrovi E, Giorgis F, *et al.* Doubly resonant porous silicon microcavities for enhanced detection of fluorescent organic molecules. Sens Actuators, B. 2009;137(2):467–70.
203. Setzu S, Létant S, Solsona P, Romestain R, Vial JC. Improvement of the luminescence in p-type as-prepared or dye impregnated porous silicon microcavities. J Lumin. 1998;80(1–4):129–32.
204. Qiao H, Guan B, Bocking T, Gal M, Gooding JJ, Reece PJ. Optical properties of II-VI colloidal quantum dot doped porous silicon microcavities. Appl Phys Lett. 2010;96(16):161106.
205. Poitras CB, Lipson M, Du H, Hahn MA, Krauss TD. Photoluminescence enhancement of colloidal quantum dots embedded in a monolithic microcavity. Appl Phys Lett. 2003;82(23):4032–4.
206. DeLouise LA, Ouyang H. Photoinduced fluorescence enhancement and energy transfer effects of quantum dots porous silicon. Phys Status Solidi C. 2009;6(7):1729–35.
207. Rossi AM, Wang L, Reipa V, Murphy TE. Porous silicon biosensor for detection of viruses. Biosens Bioelectron. 2007;23(5):741–5.
208. Krismastuti FSH, Pace S, Voelcker NH. Porous silicon resonant microcavity biosensor for matrix metalloproteinase detection. Adv Funct Mater. 2014;24(23):3639–50.
209. Levitsky IA, Euler WB, Tokranova N, Rose A. Fluorescent polymer-porous silicon microcavity devices for explosive detection. Appl Phys Lett. 2007;90(4), 041904–1 - -3.
210. Moadhen A, Elhouichet H, Oueslati M, Férid M. Photoluminescence properties of europium-doped porous silicon nanocomposites. J Lumin. 2002;99(1):13–7.
211. Moadhen A, Elhouichet H, Canut B, Sandu CS, Oueslati M, Roger JA. Evidence for energy transfer between Eu3+ and Tb3+ in porous silicon matrix. Mater Sci Eng B. 2003;105(1–3):157–60.
212. Elhouichet H, Othman L, Moadhen A, Oueslati M, Roger JA. Enhanced photoluminescence of Tb3+ and Eu3+ induced by energy transfer from SnO2 and Si nanocrystallites. Mater Sci Eng B. 2003;105(1–3):8–11.
213. Koenderink AF. On the use of Purcell factors for plasmon antennas. Opt Lett. 2010;35(24):4208–10.
214. Jenie SNA, Du Z, McInnes SJP, Ung P, Graham B, Plush SE, et al. Biomolecule detection in porous silicon based microcavities via europium luminescence enhancement. J Mater Chem B. 2014.
215. Lee H-K, Cao H, Rana TM. Design, microwave-assisted synthesis, and photophysical properties of small molecule organic antennas for luminescence resonance energy transfer. J Comb Chem. 2005;7(2):279–84.
216. Bisswanger H. Enzyme assays. Perspect Sci. 2014;1(1–6):41–55.
217. Ispas CR, Crivat G, Andreescu S. Review: recent developments in enzyme-based biosensors for biomedical analysis. Anal Lett. 2012;45(2–3):168–86.
218. Ouyang H, Christophersen M, Viard R, Miller BL, Fauchet PM. Macroporous silicon microcavities for macromolecule detection. Adv Funct Mater. 2005;15(11):1851–9.
219. Jenie SNA, Prieto-Simon B, Voelcker NH. Development of l-lactate dehydrogenase biosensor based on porous silicon resonant microcavities as fluorescence enhancers. Biosens Bioelectron. 2015;74:637–43.